PLOS ONE

RESEARCH ARTICLE

Changes in the three-dimensional microscale topography of human skin with aging impact its mechanical and tribological behavior

Juan G. Diosa[1], Ricardo Moreno[1], Edwin L. Chica[1], Junes A. Villarraga[1], Adrian B. Tepole[2,3]*

1 Mechanical Engineering Department, Universidad de Antioquia, Medellín, Colombia, **2** School of Mechanical Engineering, Purdue University, West Lafayette, Indiana, United States of America, **3** Weldon School of Biomedical Engineering, Purdue University, West Lafayette, Indiana, United States of America

* abuganza@purdue.edu

Citation: Diosa JG, Moreno R, Chica EL, Villarraga JA, Tepole AB (2021) Changes in the three-dimensional microscale topography of human skin with aging impact its mechanical and tribological behavior. PLoS ONE 16(7): e0241533. https://doi.org/10.1371/journal.pone.0241533

Editor: Jose Manuel Garcia Aznar, University of Zaragoza, SPAIN

Received: November 3, 2020

Accepted: May 11, 2021

Published: July 9, 2021

Data Availability Statement: Data related to this manuscript are held in a public repository https://bitbucket.org/abuganzatepole/skinmicrorelief3dmodel.

Funding: This work was carried out under support of Colombia Ministry of Science, Technology and Innovation MINICIENCIAS (COLCIENCIAS Doctorado Nacional 647 -2014/Universidad de Antioquia). The financial support of the Universidad de An- tioquia is also gratefully acknowledged. This work was also partially supported by award CMMI

Abstract

Human skin enables interaction with diverse materials every day and at all times. The ability to grasp objects, feel textures, and perceive the environment depends on the mechanical behavior, complex structure, and microscale topography of human skin. At the same time, abrasive interactions, such as sometimes occur with prostheses or textiles, can damage the skin and impair its function. Previous theoretical and computational efforts have shown that skin's surface topography or microrelief is crucial for its tribological behavior. However, current understanding is limited to adult surface profiles and simplified two-dimensional simulations. Yet, the skin has a rich set of features in three dimensions, and the geometry of skin is known to change with aging. Here we create a numerical model of a dynamic indentation test to elucidate the effect of changes in microscale topography with aging on the skin's response under indentation and sliding contact with a spherical indenter. We create three different microrelief geometries representative of different ages based on experimental reports from the literature. We perform the indentation and sliding steps, and calculate the normal and tangential forces on the indenter as it moves in three distinct directions based on the characteristic skin lines. The model also evaluates the effect of varying the material parameters. Our results show that the microscale topography of the skin in three dimensions, together with the mechanical behavior of the skin layers, lead to distinctive trends on the stress and strain distribution. The major finding is the increasing role of anisotropy which emerges from the geometric changes seen with aging.

Introduction

Our perpetual interaction with the environment is mediated by the skin, the largest organ in our body [1, 2]. Contact with the objects in our surroundings enable us to understand and interpret what we touch, from perceiving shape and texture, to manipulating objects dexterously [3–6]. Unfortunately, mechanical interaction between the skin and the environment can

1916668 to Adrian Buganza Tepole. The funders had no role in study design, data collection and analysis, decision to publish, or preparation of the manuscript.

Competing interests: No authors have competing interests.

also lead to injury, from superficial abrasion to chronic wounds [7–9]. This is especially true in situations in which there is constant contact, cyclic relative motion, and large tangential and normal forces applied to the skin [10, 11]. A primary example of this kind of scenario is the interaction between skin and prostheses [12–15]. Another example is pressure sore initiation in individuals who are bed- or wheelchair-ridden [16–18]. Among other factors, such as ischemia and inflammation [19, 20], friction between the skin of these individuals and textiles or common materials used in wheelchair or prostheses design can contribute to abrasion and skin damage, paving the way for more serious chronic wounds [7, 21–23]. Other applications for which anticipating skin pressure and friction are important include the design of shoes and clothing for diabetic individuals, wearable robots for rehabilitation, exoskeletons for soldiers, and sports equipment [24].

Skin has remarkable mechanical properties that enable its function. This organ is strong and tough yet flexible. It operates physiologically in the large deformation regime and shows a highly nonlinear stress-strain response. The frictional behavior of human skin at the tissue scale (in the order of cm) is affected by several variables including age [25, 26], anatomical region [27–29], contact material [30], type of contact [5, 31], environmental conditions [6, 26, 28], and hydration of the tissue [16, 32]. However, to discriminate between the relative contributions of these factors, it is advantageous to zoom in to the mesoscopic scale, in the order of hundreds of μm to a few mm. At this scale, the friction between the skin and a given material depends strongly on the inherent mechanical features seen at this scale: the mechanical properties of the different skin layers, the deformation of the tissue during contact, and the topography of the skin, also referred to as microrelief [33, 34]. However, our knowledge of skin friction at this mesoscopic scale has several, important gaps. In particular, here we are chiefly interested in elucidating how changes of skin three-dimensional (3D) structure with aging may alter the mechanical and frictional behavior of this tissue.

For such a thin structure, the skin has a fascinating architecture. The tissue can be divided into three layers. At the top there is the epidermis, below that the dermis, and the hypodermis is the bottom layer, connecting the skin to the underlying muscle [35, 36]. The sublayer of the epidermis right above the interface with the dermis is populated by keratinocyte cells. As these cells proliferate and differentiate they move up through the epidermis. Some of the changes in keratinocyte cells associated with differentiation include accumulation of keratin, gradual disintegration of organelles, and eventually cell death [37, 38]. In fact, the outermost sublayer of the epidermis, the stratum corneum (SC), is made out of dead cells called corneocytes, which are constantly released to the environment via desquamation [39]. The biological changes during cell differentiation in the epidermis have corresponding changes in mechanical properties. Commonly, two different mechanical responses are distinguished for the top layer of the skin, that of the living part of the epidermis, and that of the SC. The middle layer of the skin, the dermis, has a completely different structure compared to the epidermis and, consequently, also shows a unique mechanical function. The dermis is a collagen-based connective tissue that is mainly responsible for the tensile properties of skin [40]. Directions of anisotropy in the dermis due to the collagen fiber architecture are associated with Langer's lines, which are the principal directions of *in vivo* pre-strain of skin [41]. Underneath the dermis, the hypodermis or subcutaneous tissue has yet a different composition and mechanical behavior. The hypodermis is made out of fat cells and tissue, serving as a loose viscoelastic attachment to the underlying muscle. Remarkably, the complex skin microstructure is packed in a thickness of only 1–3mm (see Fig 1).

In addition to its organization across the thickness, the top surface and the interfaces between the skin layers also show a non-trivial geometry. The interface between the epidermis and the dermis is a two-dimensional surface with a wave-like pattern of peaks and valleys

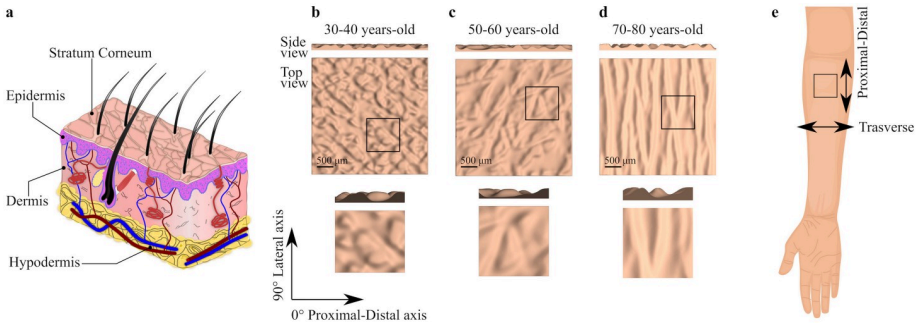

Fig 1. Human skin anatomy and topography. a) Schematic of human skin layers, **b**) 30–40 years-old topography, **c**) 50–60 years-old topography,**d**) 70–80 years-old topography. Three-dimensional surface geometries are reconstructed based on the work by Zahonuani et al [42]. e) Anatomical site information of the reconstructed three-dimensional surfaces.

https://doi.org/10.1371/journal.pone.0241533.g001

called the rete ridges [43–45]. The outermost surface of the skin also shows an intricate microscale topography or microrelief. This topography is usually characterized by furrows and plateaus on the surface of the skin. These features are delimited by different lines classified by their width and depth into primary, secondary, and in some cases even tertiary and quaternary lines [45–47]. The primary lines are the deepest and correspond to the visible polygonal plateaus on the skin surface. Primary lines help to control sebum quantity and movement of sweat. The secondary lines go across the plateaus formed by the primary lines. The orientations of the primary and secondary lines are also associated with the underlying skin anisotropy and Langer's lines [41]. The topography of the skin surface, mainly the area of the plateaus and the direction of the primary lines, has been identified as a key for skin's frictional response [48, 49].

The skin, like most biological tissues, shows inherent variability in structure and mechanical properties within and across individuals. For instance, even focusing on the skin of an individual, there is variation with respect to anatomical location and the environment conditions. Hydration and swelling of the corneocytes through water absorption [50] leads to reduction of the apparent stiffness of the SC by orders of magnitude compared to the baseline physiological state [39, 51]. Those changes in the SC mechanics are reflected in a broad range of values for the friction coefficient between skin and different materials [25, 30, 52, 53]. For example Klaassen et. al. have found that a change in relative humidity from 40% to 80% leads to up to a two-fold increase in the friction forces [52, 54].

Like all living tissues, skin does not remain unchanged throughout our lifetime, but it adapts its structure and mechanical behavior based on sun exposure, mechanical cues, disease, and aging [46, 47, 55]. In particular, dramatic changes of skin microrelief characteristics with aging have been reported (see Fig 1) [42, 46]. The main trends are changes in the direction, depth and width of the primary lines [42, 47, 56]. In consequence the plateaus area increases with aging [57, 58]. Changes in morphology, composition, and mechanical properties have also been reported with aging. For instance, the dermis becomes thinner, the tissue becomes more compliant under small deformations, but it is stiffer at large deformations [59, 60].

Experimentally, the coefficient of friction for human skin in contact with different materials is usually evaluated as the ratio between the recorded tangential and normal forces. These measurements have been almost entirely restricted to the macroscopic scale (on the order of cm). The results from such experiments have shown that the frictional response of human skin at this scale cannot be accurately described by common models such as Amontons—Coulombs [3, 5, 61, 62]. Several other, more complex descriptions have been proposed, including

statistics regression models [25, 26], power laws [3, 28, 37, 53], adhesion models [63] and others [64]. These efforts are focused on capturing the macroscopic scale phenomena. Yet, a major gap in our knowledge is the limited understanding of the role played by the mesoscale structure and mechanical response in producing the observed friction at the larger spatial scales. It is extremely difficult to experimentally dissect the fundamental mechanisms occurring at the mesoscale because of the inherent challenge in measuring the force and contact area distributions with a fine enough resolution in relevant scenarios. Instead, high-fidelity computational models can help bridge this gap. For example, Leyva-Mendivil et. al. [33, 34] used a two-dimensional model of skin to analyze the changes in friction coefficient due to the influence of the rigidity of the SC, indenter radius, indentation depth, and local coefficient of friction. The results of these studies show the importance of the skin surface topography and SC stiffness. Yet, even though the surface of the skin has a rich set of features in 3D, and the geometry of skin is known to change with aging, the effect of these features on the mechanical and tribological response of skin has not been thoroughly investigated.

In this paper we build a detailed 3D finite element model of skin in contact with a spherical indenter in order to elucidate the effect of microrelief changes with aging. Realistic computational models of skin mechanics are now possible due to the comprehensive characterization and constitutive modeling of human skin over the past few decades. Skin has been studied with uniaxial, biaxial [65, 66], multiaxial [67], bulge [68], suction [69], and indentation tests. Several constitutive models have been proposed pertinent to different applications, loading conditions, and time scales. For example, linear [70], viscoelastic [71, 72], multiphasic [1], and hyperelastic [73, 74] constitutive models have been used. There have also been efforts to distinguish between the mechanical behavior of the different skin layers [75]. We use constitutive models and parameters from experimental testing of skin under indentation [76, 77].

Methods

We create detailed 3D finite element models of skin based on reported measurements of the skin microscale topography available in the literature [42, 49, 57, 78]. In particular, the work by Zahouani et. al. has led to a thorough characterization of the changes in skin microrelief with aging, with geometric features on the order of 160 μm. We use their data to reconstruct surfaces in 3D, and then extrude these surfaces computationally to get the solid 3D geometry.

Reconstruction of skin surface geometries

We base our models on the 3D confocal microscope analysis of human skin topography by Zahouani et al [42]. The z-height contours of the left forearm skin of 3 representative subjects were processed, one contour from each of the following age groups: 30–40, 50–60, and 70–80 years-old. A section of 3.5 mm x 3.5 mm from each image is selected and pre-processed on GIMP 2.10. To deal with the excessive noise in the contour images, which would result in unrealistic surface profiles, we apply a 5x5 pixel Gaussian blur filter and scale all the images to 100 x 100 pixels using a cubic interpolation method. A Matlab ® (version R2018a; The MathWorks Inc., Massachusetts, USA) script then reads from the PNG file the pixel color and assigns a height value based on the contour scale from the original images [42]. The surfaces built in this manner are further smoothed out by applying a Gaussian filter with $\sigma = 0.75$ pixels to relocate the remaining extreme outlier heights. The surfaces capture the distinct geometric features of different ages. We analyze the topography of each age group using ImageJ 1.52a to determine the direction of the primary skin lines. In Fig 1, the 0˚ direction is aligned with the proximal-distal axis of the arm, from the elbow to the wrist, and the 90˚ direction is aligned with the lateral axis. Two different quadrants are analyzed, the first one between 0˚ to 90˚ and

the second one between 90˚ and 180˚. Primary lines in the images are identified manually in both quadrants separately, the direction of these lines is saved, and the median from five measurements for each age are computed. In the 30–40 years-old geometry, the primary lines show are oriented at 43.3˚ and 136.5˚; in the 50–60 years old case the lines are oriented at 46.3˚ and 103.9˚; and in the 70–80 years-old skin the primary lines are oriented at 81.4˚ and 100.4˚.

Generation of 3D finite element meshes

We create a finite element mesh for each of the geometries with a custom Matlab script. The mesh has 12 elements through the thickness, with element-element interfaces placed so as to capture four anatomical layers: stratum corneum (SC), viable epidermis, dermis and hypodermis, with thicknesses 0.02mm [13, 51, 79], 0.05 mm [76], 0.84 mm [76] and 2 mm [80], respectively. Analogous to the top surface topography, the epidermis-dermis interface shows a similar profile [36, 79, 81], but the subsequent interfaces between skin layers can be assumed almost flat [33, 46, 76]. Hence, we apply linear smoothing of the surface profile as we extrude the mesh through the thickness. To avoid boundary effects in the simulations of the skin in contact with the spherical indenter, we embed the mesh generated with our Matlab code into a larger domain (Fig 2a). The extension of the skin model is created on preview 2.1 (MRL The University of Utah, MBL Columbia University). This additional portion of the domain also has four anatomical layers with different properties but lacks the surface topography. To match the nodes at the interfaces of both meshes, a transition region is also prescribed in the Matlab-generated mesh. The indenter used in this study is a smooth hemisphere of 5mm diameter. The models created have an average of 367,522 nodes and 340,065 Hex8 elements.

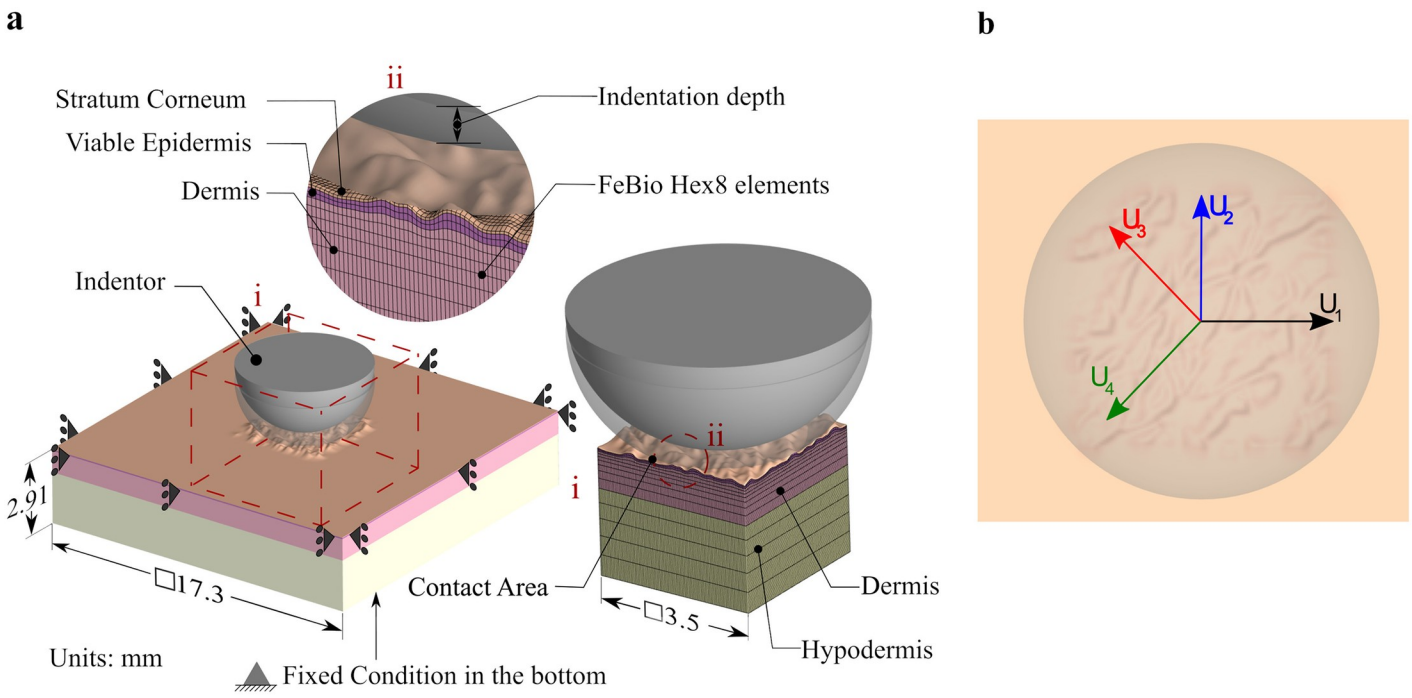

Fig 2. Finite element model creation. a) Indentation step. The domain is more than three times larger than the indenter radius to minimize boundary effects. The spherical indenter interacts with a portion of the domain that has a detailed microrelief geometry, shown in the zoomed region (i). The mesh consists of Hex8 elements, with 12 elements through the thickness to capture the four layers of skin. Additional detail is shown in the subpanel (ii). **b**) Indenter directions of movement in displacement step are decided based on the anatomical axis (lateral U_1, proximal-distal U_2) as well as perpendicular to the primary skin lines (U_3, U_4).

https://doi.org/10.1371/journal.pone.0241533.g002

Mechanical behavior of skin

The viable epidermis, dermis and hypodermis are assumed to follow the Ogden hyperelastic constitutive relation, with material parameters obtained from the literature (Table 1) [76]. The SC is modeled as a neo-Hookean solid. To investigate the influence of the SC hydration on its mechanical behavior, two different properties are considered. The low rigidity represents the behavior of the SC under wet conditions [33, 34, 46, 82]. In the dry condition, SC is up to sixty times stiffer than in the wet condition [46, 82]. The spherical indenter is modeled as a rigid body.

Age-related changes in mechanical properties and thickness

While the main focus in this study is the effect of the skin microrelief, mechanical properties of skin have also been reported to change with age. Overall there is a thickness reduction of the whole skin with aging, and in particular the dermis [45, 59]. We thus performed additional simulations in which we reduced by 50% the dermal thickness of the 50–60 and the 70–80 microrelief models. According to reports of change in dermis mechanical properties with aging [59, 60, 83, 84], which suggest that there is more compliance in the dermis at small stretches but stiffer response at larger stretches, we considered two additional values of the shear modulus of the dermis with respect to the parameter in Table 1. In one case we reduced the shear modulus of the dermis by half, and in the other case we considered twice the value in Table 1.

Boundary and contact conditions

The bottom surface of the model is fixed in all directions to reflect the attachment of the subcutaneous adipose tissue to the underlying fascia, which can be considered as a rigid attachment in this context [34, 76, 85]. The lateral surfaces of the model satisfy symmetry conditions in their respective planes. The movement of the indenter is divided into two steps: static indentation following by dynamic contact. We consider an indentation depth of 500 μm (Fig 2a). After the tip reaches the prescribed depth, the indenter moves horizontally along one of four different directions: U_1, parallel to the global x axis which is the proximal-distal axis of the forearm; U_2, parallel to the global y axis which is the transverse axis; U_3 or U_4, normal to the direction of the primary lines determined for each age (Fig 2b). We model the contact between the indenter and the skin using the *sliding elastic contact* formulation in FeBio with the augmented Lagrangian strategy. In this study we model two cases: we perform simulations with frictionless contact as a control; we then set the local coefficient of friction to be $\mu_l = 0.2$. For further control, we generate equivalent models but without the microrelief, i.e. flat geometries. We compute the coefficient of friction as the ratio between the tangential forces, f_t and f_b (collinear and orthogonal to the indenter movement respectively), and normal forces, f_n [86],

$$\mu_g = \frac{\sqrt{f_t^2 + f_b^2}}{f_n} \tag{1}$$

Table 1. Material parameters for the different human skin layers [33, 46, 76].

Layer	Parameter 1 [MPa]	Parameter 2[-]
SC (Dry)	E = 360	$\nu = 0.48$
SC (Wet)	E = 6	$\nu = 0.48$
Viable Epidermis	$\mu = 7.74823$	$\alpha = 2.4291$
Dermis	$\mu = 0.0205$	$\alpha = 3.2999$
Hypodermis	$\mu = 0.0094$	$\alpha = 4.0319$

https://doi.org/10.1371/journal.pone.0241533.t001

Multivariate regression analysis

In order to quantify the influence of each factor from the simulation on the resulting coefficient of friction, we do a multivariate analysis based on generalized linear regression using R 3.6.1 (R Foundation). The parameters are codified as follows: for the age group we use 1 for the 30–40 year-old geometry, 2 for 50–60 year-old case, and 3 for the 70–80 year-old geometry; for the material properties of the skin, 1 codifies wet and 2 is used for dry; finally, the codes for the different directions are 1, 2, 3 and 4 for U_1, U_2, U_3 and U_4 respectively. The regression is thus summarized as

$$\mu_g = intercept + \beta_1 X_1 + \cdot + \beta_n X_n \tag{2}$$

where the values of the dependent factor μ_g are the average coefficient of friction during the displacement step of the finite element simulation.

Results

We run a total of 38 analyses (26 with full thickness and 12 with the reduced thickness) using FeBio 2.8.2 (MRL The University of Utah, MBL Columbia University) [87]. The postprocesing stage is carried out in PostView 2.3 (MRL The University of Utah, MBL Columbia University).

Strain contours during indentation are sensitive to SC mechanical properties

Representative results from the indentation analysis are illustrated in Fig 3, where the E_{33} component of the Green Lagrange strain is plotted for a cross section. The Fig shows the results for both dry and wet SC conditions and for three different ages. The flat control is also shown. The maximum magnitudes in E_{33} occur in the dermis region under all conditions. The contours of the normal strain resemble Hertzian theory; however, even in the flat control, the different mechanical properties across skin layers contribute to the distortion of the strain contours. There is also an expected boundary effect from the fixed displacements imposed at the bottom of the model, in contrast to Hertzian stress contours which are based on the contact between an indenter and an elastic half-space.

In Fig 4a and 4b, both the E_{33} and E_{13} components of the Green Lagrange strain are plotted along the skin thickness for dry or wet SC conditions and for the different geometries. The plots correspond to elements directly below the center of the indenter. The normal strains are very similar in all cases, whereas the shear strain profiles show significant variation across simulations. The greatest differences in the shear strain between different cases occurs near the top layers of the skin, with E_{13} decaying to zero through the dermis and the hypodermis. These variations are related to the surface topography since, as can be seen in Fig 4a, the shear strains in the flat geometries are small and do not show oscillations across the thickness. For the detailed geometries, shear strains tend to reach higher magnitude in the wet SC cases compared to simulations with dry SC properties, although this is not always the case. It should also be noted that, even though the microrelief induces shear strains in the skin, these strains are an order of magnitude lower compared to the normal strains depicted in Fig 4b. The normal strain E_{33} increases rapidly in magnitude in the epidermis, and then continues to increase in magnitude over the dermis, before going smoothly back to zero over the hypodermis. The plot is consistent in all cases, with small variations and no evident trend.

Therefore, Figs 3 and 4 together indicate that strains in the skin during indentation are mostly normal rather than shear and that the strain profile resembles a Hertzian contour as a consequence of the sliding contact interface. However, we also see that the different stiffness

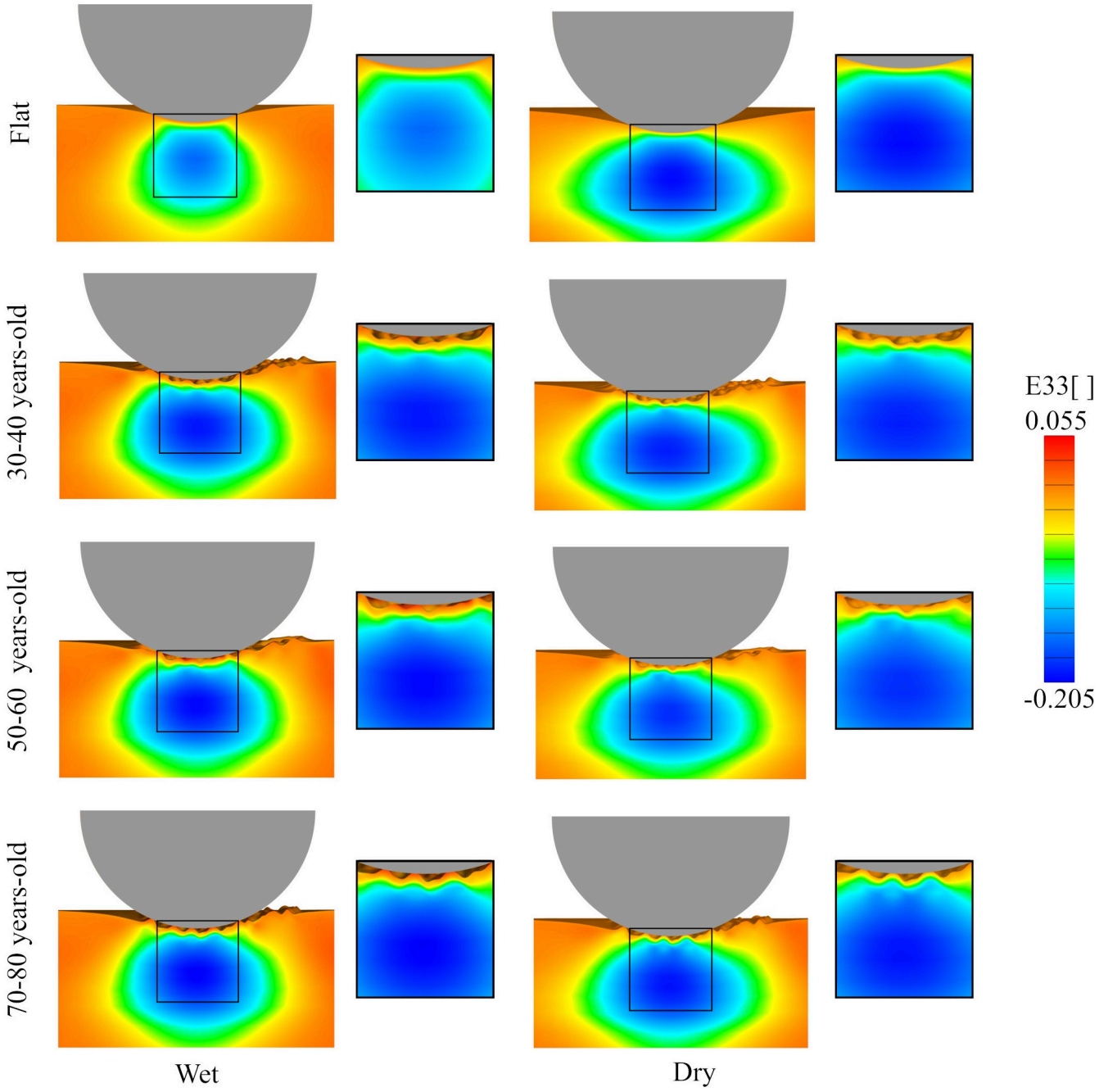

Fig 3. Normal strain contours due to indentation. Component E_{33} of the Green Lagrange strain tensor for different SC condition (wet or dry) for the three different microrelief geometries and the flat control. The strain resembles Hertzian contours. However, even in the flat control, the strain contours are distorted by the changing mechanical properties across skin layers as well as boundary conditions associated with the finite thickness of the skin. The wetness of the SC has a noticeable effect. As the SC dries, its stiffness increases, and the corresponding contours extend over a larger region in the underlying skin layers. The microrelief further contributes to the distortion of the strain contours compared to the flat geometry. In particular, the contours become asymmetric and localized around the features of the surface topography.

https://doi.org/10.1371/journal.pone.0241533.g003

across skin layers dictate the deformation across the thickness, with a sharp increase in compression in the epidermis and a maximum compression in the dermis. These observations highlight the importance of considering individual skin layer properties when understanding this tissue's mechanical behavior.

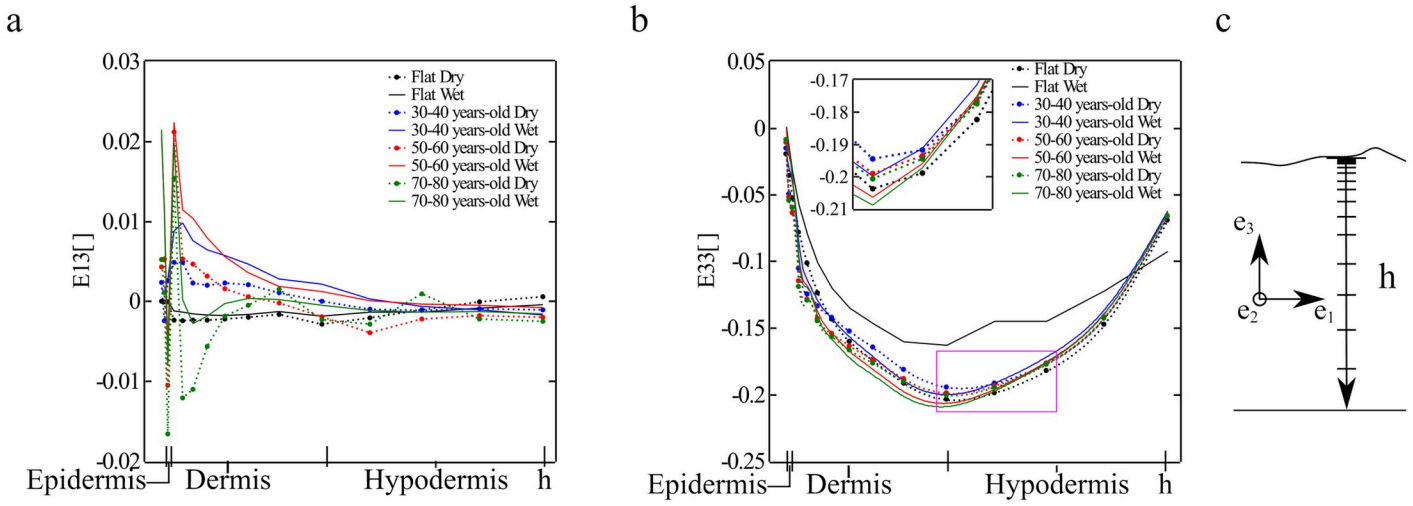

Fig 4. Strain through the skin thickness following indentation. Components of the Green-Lagrange strain plotted across the skin thickness right underneath the indenter for the different age topographies and different SC condition (wet or dry): **a**) E_{13}, **b**) E_{33}. The coordinate system is shown in **c**.

https://doi.org/10.1371/journal.pone.0241533.g004

Influence of age-related changes in the dermis mechanical properties and thickness

Fig 5a shows the E_{33} Green-Lagrange strain component for the two oldest microrelief geometries, with a reduced thickness of 50% with respect to the original model, as well as three different shear modulus values for the dermis. Only the dry SC condition is shown in the main text, additional simulations with the different values of the shear modulus for both wet and dry SC properties are shown in the Supplement. The change in thickness produces less elliptical and more cone-like shapes of the E_{33} contours in comparison to Fig 3. Small variations with respect to the shear modulus are observed. To better visualize the change in strain across the thickness and also at different spatial locations with respect to the indenter, components E_{33} and E_{13} for the 50–60 years-old model are shown in Fig 5b. For each position, the normal strains E_{33} have very similar behavior for the three values of the dermis shear modulus, whit minor differences in the epidermis and dermis zones. The trends also align with the simulations depicted in Fig 4. The shear strain profiles show significant spatial variation. Right below the center of the indenter the shear strains are small, but they increase for locations away from the center line and toward the edge of the indendet region. Additionally, shear strains are larger for the softer dermis properties.

Influence of aging topography on the surface stress during indenter movement

Following the indentation step, the indenter is displaced along one of the directions shown in Fig 2. First, we focus on the displacement along U_1 and compare the effect of SC properties and the influence of changing geometry with aging. Fig 6 shows the contours of maximum principal stress and maximum shear at the top surface for the three different aging geometries as well as the flat control, and for the two SC conditions. The maximum stress values remain similar for the three different aging topographies, but change noticeably with the change between dry and wet conditions. The changes in principal stress contours for the flat geometry are striking. For the wet case, the SC stiffness is even lower than the underlying epidermis, and the principal stress at the surface of the indented region is negligible. In fact, the greatest

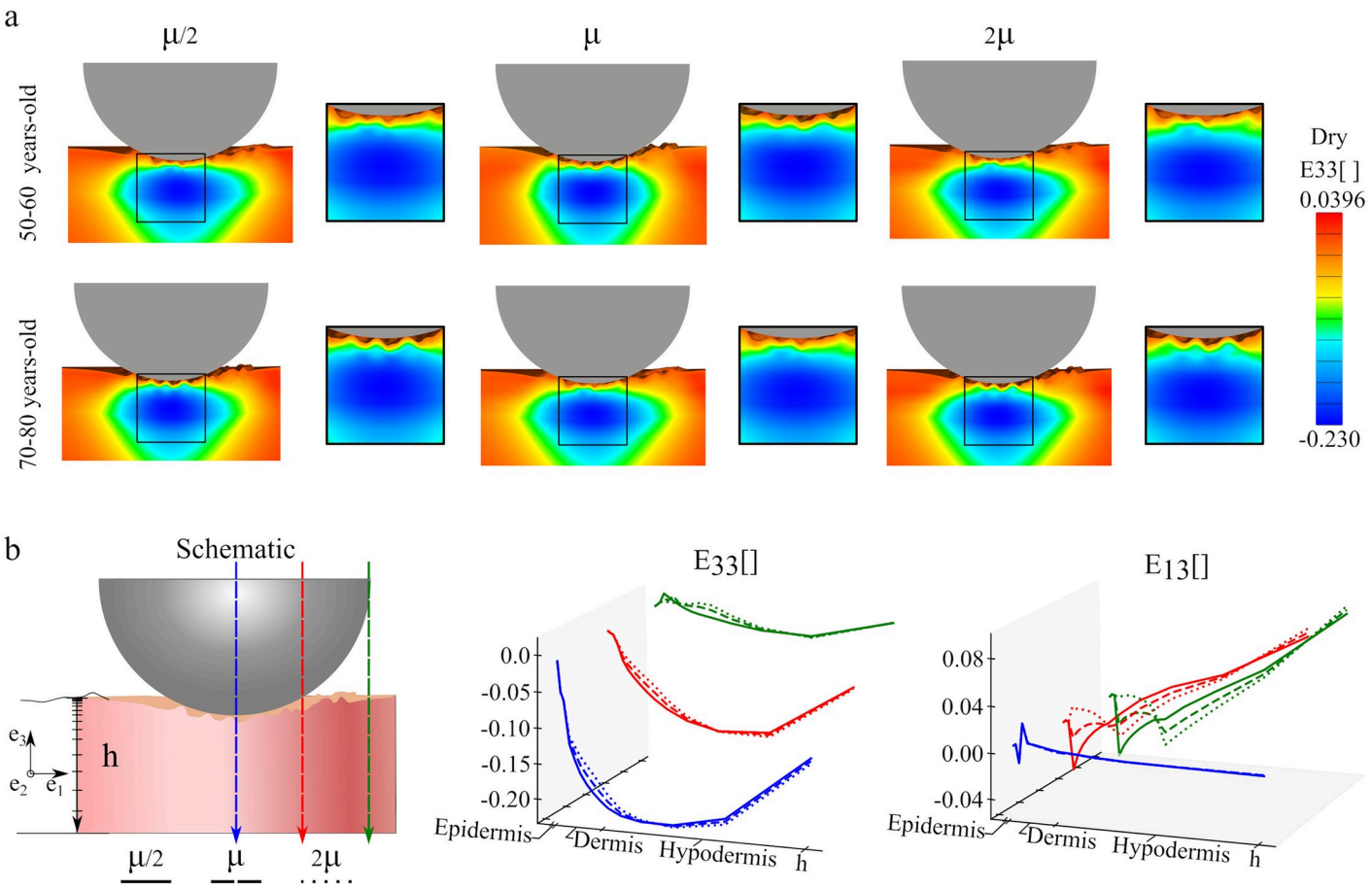

Fig 5. Effect of dermal thickness and stiffness on the mechanical response to indentation. Contours of the Green Lagrange strain components E_{33} and E_{13} for the two oldest microrelief geometries for the reduced thickness model with dry SC condition, and for three values of the shear modulus for the dermis (**a**). Components E_{33} and E_{13} of the Green Lagrange strain plotted across the skin thickness in three different positions underneath the indenter (**b**).

https://doi.org/10.1371/journal.pone.0241533.g005

principal stress at the surface occurs towards the edge of the indented region. As the SC becomes stiffer, the principal stress contour achieves the maximum at the center of the indented region and decreases away from the indenter. This feature is not observed in the geometries with microrelief.

In the realistic geometries with microrelief, the maximum value of the stress remains relatively unchanged with aging for a given SC condition, with wet SC leading to smaller stress at the surface compared to the dry SC, as expected. However, the most relevant results from the simulations with realistic topography are the patterns of stress distribution over the top surface of the skin due to aging-associated geometric changes. In all cases, the stress is greater in the peaks and plateaus which are in contact with the indenter, and less in the valleys defined by primary and secondary lines, which are not in direct contact with the indenter. Observations of the geometric changes in skin topography with aging translate directly into the observed stress profiles. The primary and secondary lines become more anisotropic with aging, and so do the regions with the peak stresses. For instance, in the 30–40 years-old geometry there is a weaving pattern of high σ_1 stresses, while in the 70–80 years-old geometry there are parallel bands of peak σ_1 stresses. The changes in maximum shear stress are less evident compare to the maximum principal stress.

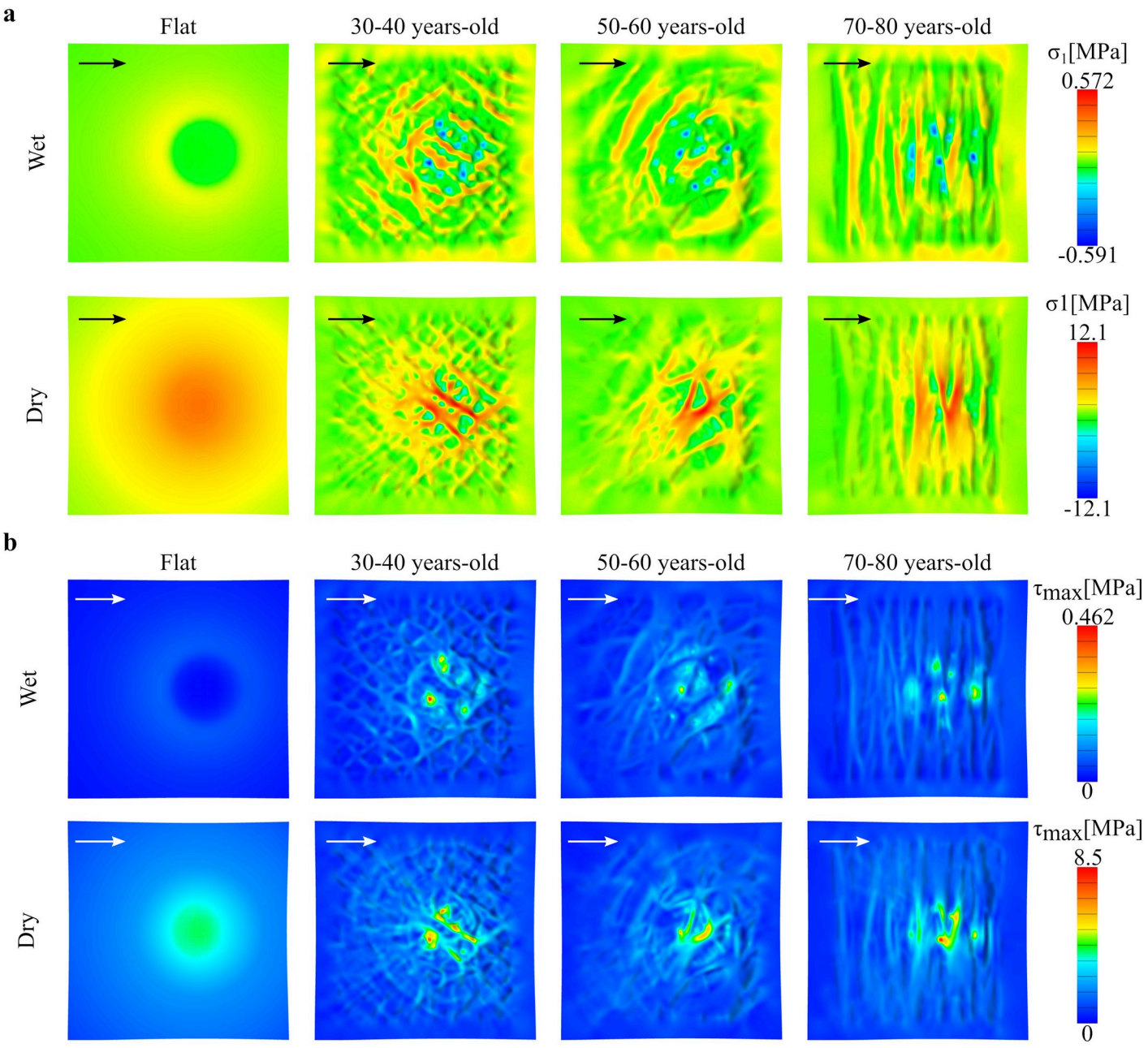

Fig 6. Stress due to indenter displacement along anatomical axes. Stress contours at the skin surface for the flat control and the three different skin topographies, for wet and dry SC conditions. The contours correspond to the final position of the indenter after it has moved in the direction U_1 for 1mm at an indentation depth of 500 μm: **a**) Maximum principal stress and **b**) Maximum shear stress.

https://doi.org/10.1371/journal.pone.0241533.g006

Table 2 lists the average contact area during the simulation for the flat control surface and the three different skin topographies for the case in which the indenter moves in the U_1 direction. There is a significant difference between SC conditions, the contact area under wet conditions is more than five times that of the dry SC case. Clearly, the softer SC in the wet case deforms more and allows for more contact area. The flat control surface has the largest contact area. The lack of asperities in this scenario allows for an ideal contact between the indenter

Table 2. Average contact area [mm^2] for the simulation with the flat skin surface and the three different skin topographies when the indenter moves in the U_1 direction.

Topography	Contact Area [mm^2]	
	Wet	Dry
Flat	9.577 e-2	2.533 e-2
30–40 year-old	7.359 e-3	1.334 e-3
50–60 year-old	1.129 e-2	2.317 e-3
70–80 year-old	1.189 e-2	2.863 e-3

https://doi.org/10.1371/journal.pone.0241533.t002

and skin. The contact area shows changes with aging. As seen in Table 2, contact area increases with aging in the microrelief geometries.

Fig 7 further helps dissect differences in skin topography when the indenter moves in the directions defined by the primary skin lines. The main difference in the magnitude of the stress is still determined by the different rigidity between dry or wet SC. Then, changes in primary skin lines further contribute to distinct patterns of stress over the skin surface, especially in the dry SC case. Due to the symmetry of the primary skin lines with respect the x-axis, there are almost no differences between U_3 and U_4. Note, however, that the lines do change with aging, showing increase alignment in the distal-proximal axis (vertical axis in Fig 7). The reorientation of the primary skin lines, in turn, leads to bands of stress instead of a concentric pattern. This feature of the stress contour was already pointed out for the movement of the indented in the anatomical axis corresponding to the proximal-distal direction U_1, and is further observed in the cases in which the indented moves perpendicular to the skin lines as seen in Fig 7. The stress contours for the indenter moving in the transverse axis U_2 are shown in the supplement (S2 Fig in S1 File). The main insight from moving the indenter in different directions is that, due to increased anisotropy of the primary skin lines, the stress contours also become anisotropic, and this effect is more pronounced in the dry SC case.

Variation in the reaction forces as a function of aging microrelief

Accompanying the changes in stress distributions, the topographical changes of the skin with aging are also reflected in the reaction forces during indenter movement, which are plotted in Fig 8. In Fig 8, F_t is the component of the reaction force in the direction of the indenter movement, F_n is the normal reaction force, i.e. normal to the horizontal plane, while F_b is the force component orthogonal to the other two directions of interest. In other words, F_b is also in the horizontal plane, but orthogonal to F_t.

The normal component of the force is very similar in all cases, oscillating between 115 and 130 mN. In comparison, the normal force corresponding to the flat geometry (grey line in Fig 8), is nearly constant at 175 mN. For context, the coefficient of friction has been assessed in experiments with normal forces ranging between 5mN and 8N [88, 89]. The normal forces obtained in this study are in the ranges of normal forces as reported experimentally [30, 44, 53]. The tangential force for the flat geometry is also nearly constant during indenter movement, at F_t = 35 mN. For the realistic geometries, the tangential force directly opposing the indenter movement oscillates around 20 mN. Interestingly, the in-plane component F_b is non-zero in the realistic geometries. In the control case of the flat geometry $F_b = 0$ as expected. In the geometries with microrelief, the force F_b oscillates between -10 and 10 mN. We remark that these forces orthogonal to the expander movement appear because the microrelief is asymmetric with respect to the plane defined by the indenter movement. From the plots in Fig 8, there is no notable difference between the directions of indenter movement. Aging does

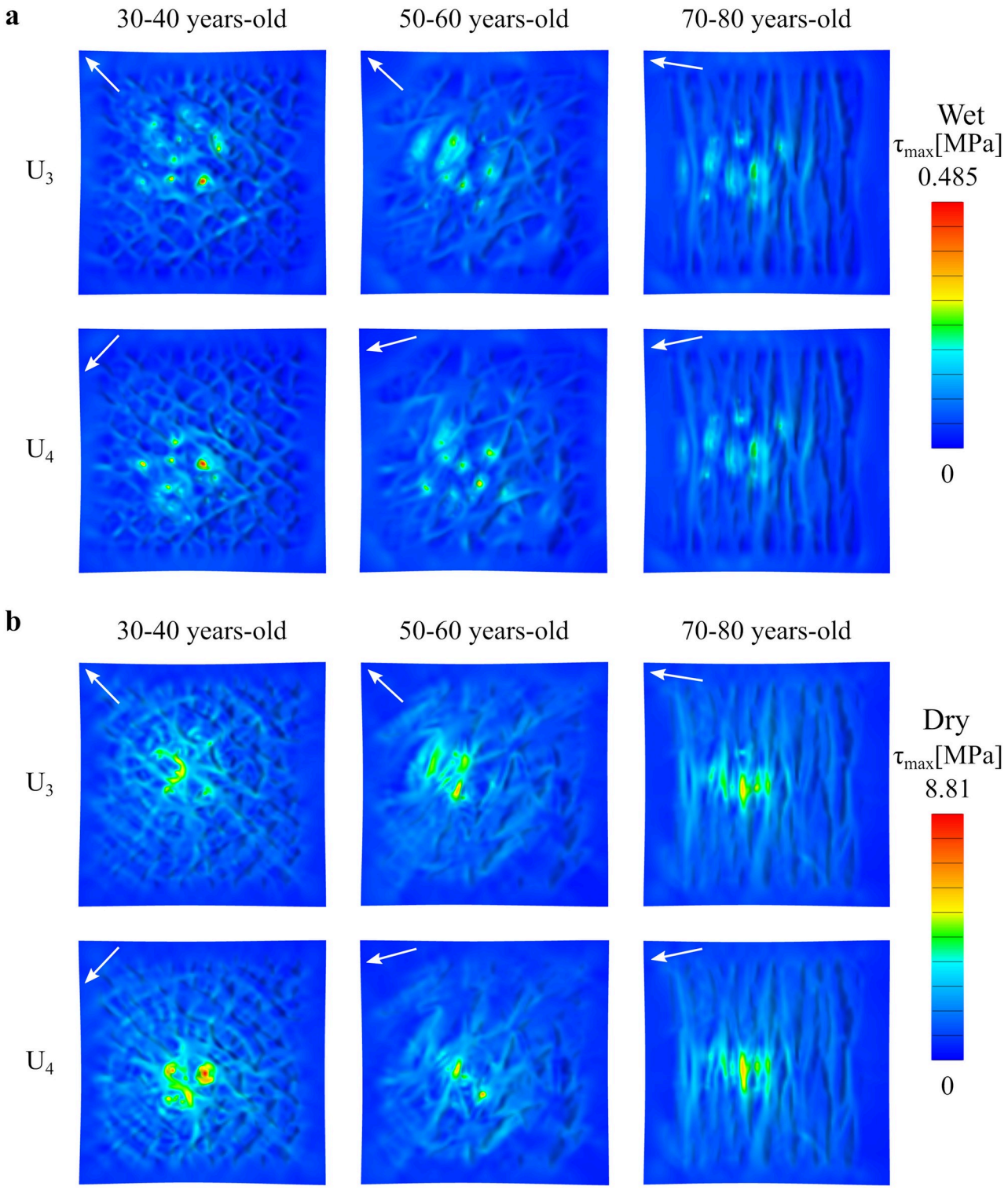

Fig 7. Stress due to indenter movement orthogonal to primary lines. Maximum shear stress contours for three different skin age topographies, for the displacement directions U_3 and U_4 given by the primary skin lines. The results correspond to: **a**)wet SC and **b**)dry SC material properties.

https://doi.org/10.1371/journal.pone.0241533.g007

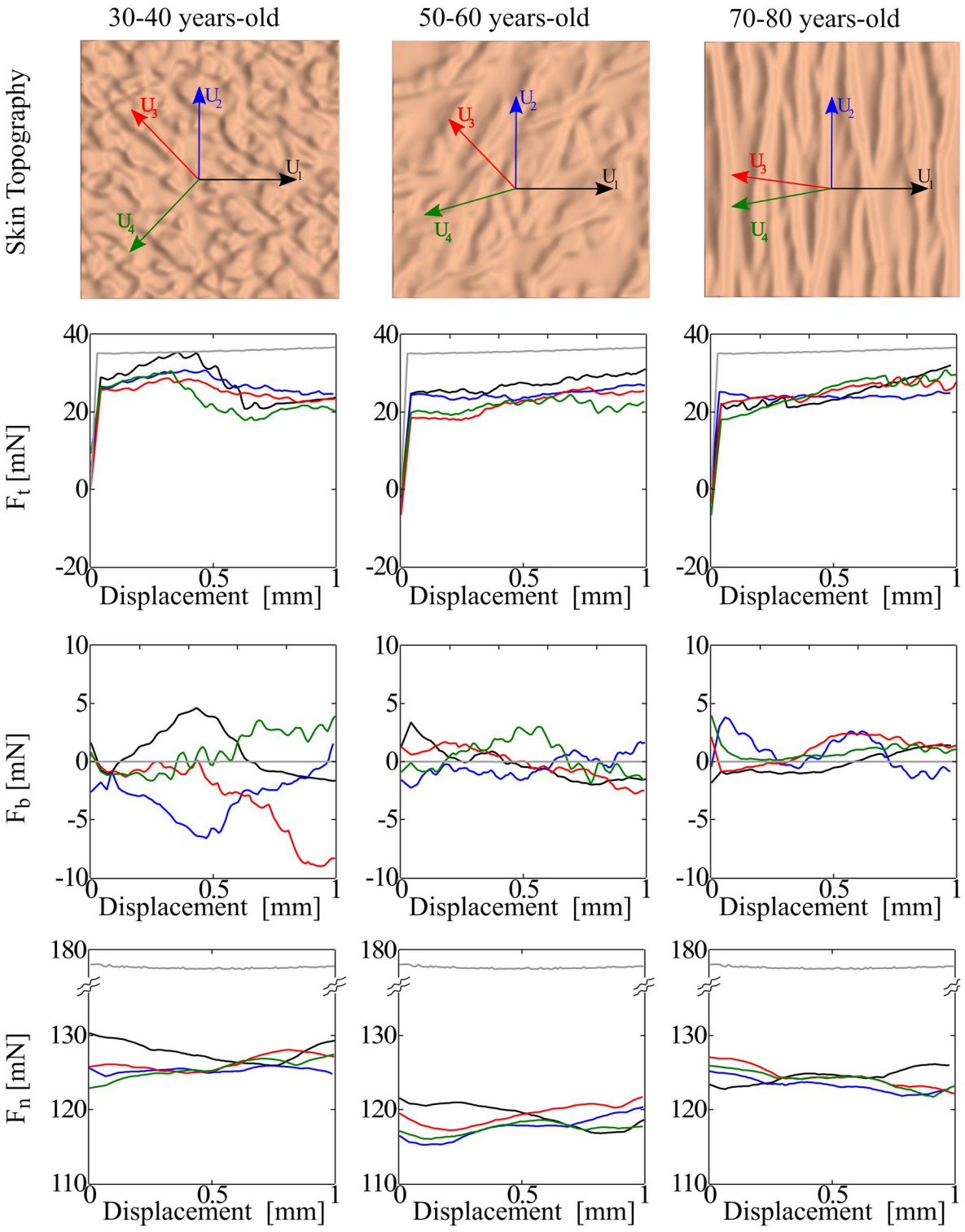

Fig 8. Normal and tangential forces during indenter movement. Behavior of in-plane (F_t and F_b), and normal (F_n) reaction forces on the indenter for three different skin age topographies and four displacement directions (black: U_1, red U_2, blue U_3, green U_4). The forces corresponding to the flat control are shown in grey. All plots correspond to the properties of the dry SC.

https://doi.org/10.1371/journal.pone.0241533.g008

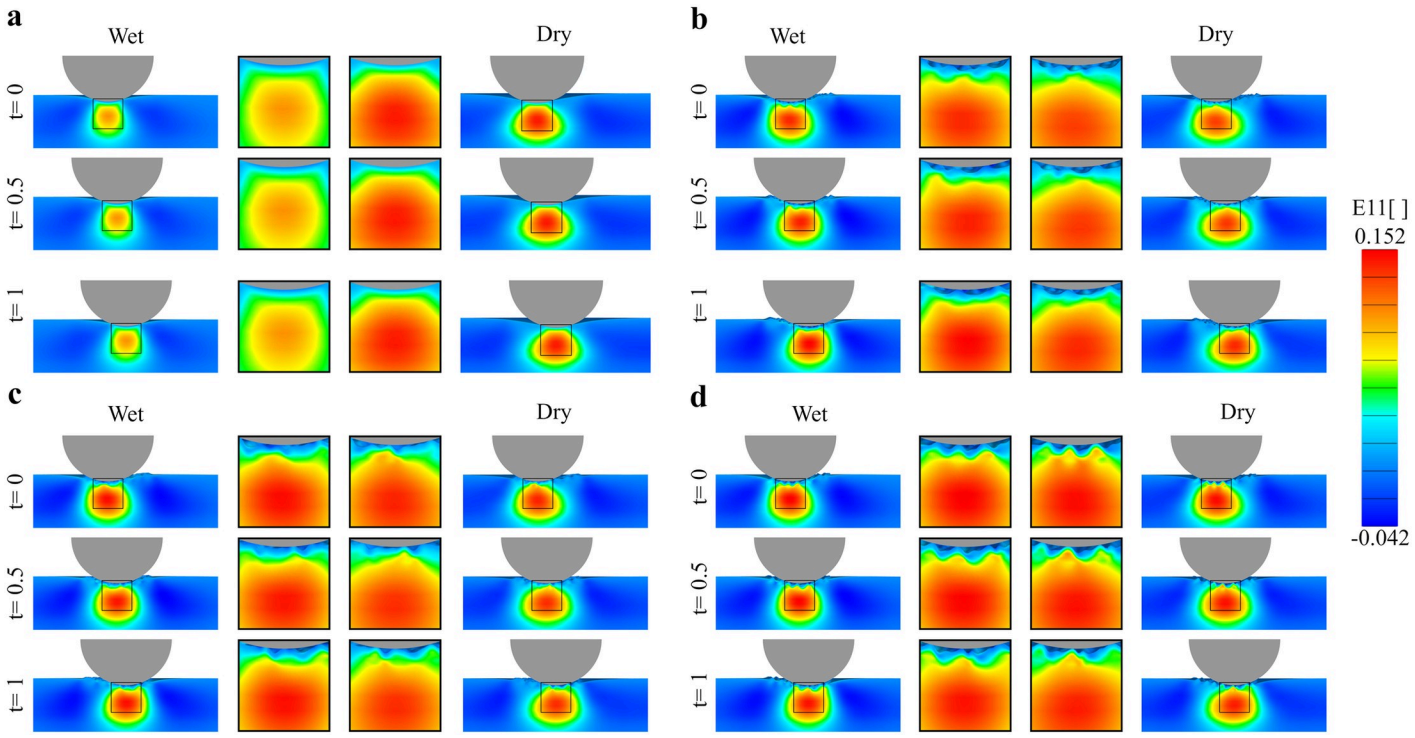

Fig 9. Strains through the skin thickness during indenter movement. Normal strain E_{11} in the direction of the indenter movement at three time points during indenter displacement (t = 0, 0.5, 1s), for the two SC conditions, and for the four different geometries:**a**) Flat, **b**) 30–40 years-old, **c**) 50–60 years-old and **d**) 70–80 years-old.

https://doi.org/10.1371/journal.pone.0241533.g009

contribute to observable trends. Changes of the microrelief with aging tend to reduce the oscillation of the tangential forces. This can be explained by the surface features with aging. In the 30–40 case, the primary lines form a weaving pattern such that the indenter crosses many obstacles as it slides on the skin. With aging, as the primary skin lines become more anisotropic there is less variation in the obstacles that the indenter has to go over.

Strain contours during indenter displacement

Fig 9 shows the E_{11} contours as the indenter moves, further clarifying the trends in the reaction forces. In the flat geometry, the E_{11} contours are unchanged as the indenter moves, which is expected and aligns with the nearly constant F_t in Fig 8 for the flat geometry. We remark that the E_{11} strain corresponds to the direction of the indenter movement. Therefore, this component of the strain can contribute to the tangential force F_t in addition to the friction force due to local contact between skin and indenter. Indeed, while the friction force between the indenter and the skin surface is a primary contributor for F_t, previous work by Tang et al, Derler et al and Leyva-Mendivil et al, on contact between indenters and soft substrates identified a deformation component of F_t [31, 34, 90]. This deformation component is characterized by a bulging ahead of the indenter as it moves. In our case, it does not appear that the skin deforms asymmetrically in the flat geometries. Consequently, the E_{11} contours appear to be symmetric with respect to the indenter movement direction. Calculating the global friction coefficient based on the F_t and F_n forces reported in Fig 8 leads to $\mu_g = 0.2043$ under dry conditions ($\mu_g = 0.2009$ on wet conditions), which is very close to the local friction coefficient $\mu_l = 0.2$. This confirms the observation that the E_{11} contours are mostly symmetric with respect to the indenter

movement and that there is a negligible deformation component for F_t in the flat geometries. The contours of E_{11} in the geometries with microrelief can help explain the variation in F_t observed in Fig 8. The overall strain contours are similar in shape and magnitude to each other, but the microrelief has two evident effects. First, the E_{11} contours are no longer constant as the indenter moves, but change due to the surface features of skin. Secondly, the contours are no longer symmetric with respect to the plane determined by the indenter movement. It can be seen in the zoom-in panels that the strains are greater in the peaks which are in contact with the indenter. Thus, for the realistic geometries, the variation in the topography leads to oscillating tangential forces given by both changes in contact area as well as the underlying mesoscale deformation. At the same time, the realistic geometries do not show a bulging ahead the indenter. Thus, we do not expect a significant deformation contribution to F_t. This is further discussed in the next section.

Global coefficient of friction

Based on the values for F_t, F_b and F_n for all simulations, we calculate the global coefficient of friction according to Eq 2. Table 3 summarizes the results. The global coefficient of friction in our simulations with microrelief is in the range $\mu_g \in [0.1845, 0.2306]$. For the flat geometry, global coefficient of friction is $\mu_g \in [0.2009, 0.2043]$ for wet to dry SC. The local coefficient of friction is $\mu_l = 0.2$. The range of μ_g for the simulations with microrelief suggests that the topography of skin contributes to the frictional response. In general the dry SC has higher values than wet SC. These results are associated with the deformation of the ridges.

Based on the result of the multivariate regression analysis with the generalized linear model for the coefficient of friction, we describe the coefficient of friction through

$$\mu_g = 0.2145 - 0.0041 X_{\text{direction}} \tag{3}$$

In this model, it is considered that the coefficient of friction follows a Gaussian distribution. The model has an adjusted generalized R–squared value of $R_{adj} = 0.16$, Ramsey's Reset for Specification for the model is 1.0183 with a p-value = 0.3792, and the residuals distribute normally according to a Jaque-Bera test with p-value = 0.9755 (see S1 Table in the S1 File). According to the regression analysis only the displacement direction of the indenter has significant influence in the coefficient of friction ($p<0.05$). The displacement direction correlates negatively with the coefficient of friction, increasing the codification value (1, 2, 3 and 4 for U_1, U_2, U_3 and U_4 respectively) the coefficient of friction is reduced, suggesting lower friction against the primary lines. The other parameters have lower or null contributions in the phenomena under the conditions analyzed in this paper.

Discussion

Understanding the frictional behavior of skin is key for the design of new technologies, from sportswear and wearable gadgets, to medical devices. The interaction between skin and other materials is complex and, due to inherent limitations with experimental setups, it is

Table 3. Coefficient of friction for three different skin topographies, four displacement directions, and two conditions of the SC.

Age	U_1		U_2		U_3		U_4	
	Wet	Dry	Wet	Dry	Wet	Dry	Wet	Dry
30–40	0.2043	0.2161	0.2009	0.2207	0.2104	0.2083	0.2085	0.1856
50–60	0.2122	0.2306	0.2052	0.2103	0.2005	0.1845	0.1977	0.1890
70–80	0.2070	0.2025	0.2023	0.1959	0.2009	0.2085	0.2008	0.2067

https://doi.org/10.1371/journal.pone.0241533.t003

challenging to resolve the effect of the skin's microrelief deformation on the measured frictional forces. Numerical investigations have offered some clues [33, 34, 46]. However, while it is known that the topography of skin changes with age, the effect of this change has not been investigated. Moreover, only two-dimensional analyses have been attempted [33, 34]. Yet, the topography of skin has features in three dimensions. To address these gaps, here we show a numerical investigation of the skin interacting with a rigid indenter accounting for the 3D features of the skin microrelief and their change with aging.

Strain contours under indentation depend on individual skin layer properties

The indentation simulations showed that the topography has a small effect on the strain contours in the skin. We recovered contours resembling classical theory of elastic contact [4]. We further confirmed the shape of the contours in idealized geometries without any microrelief. The most important factor influencing the deformation of skin under the indenter was the presence of individual layers with different mechanical properties. Indeed, the need to consider individual skin layers has been advocated by many, particularly for the type of loading present during indentation [1, 2, 76, 91, 92]. Furthermore, it has been reported in the literature that the change in humidity has a marked effect on the mechanical properties of the outermost layer, the SC. The parameters used here to represent wet and dry SC are based on measurements reported in the literature. However, there is considerable variance in reported SC properties [93–95]. Our parameters are near the extremes of the ranges found in the literature. Consequently, our simulations should be considered as representative of these extremes. Additional simulations for an intermediate value SC stiffness are shown in the Supplement. These additional results show a response in between the cases shown in the main text, as expected. Our results show that the stiffening of the SC leads to a change in the distribution of the strains over a larger region, but that the magnitude of the strains remains relatively unchanged with respect to the softer SC. It remains to test whether other static loading scenarios relevant to the skin physiology would be also visibly affected by the change in SC properties and the consideration of the other skin layers. For instance, pressure ulcers form when the skin is subject to compressive loading, particularly near bony prominences [7, 9, 16, 96, 97]. Our work in developing a detailed 3D model of skin including individual layer properties can therefore be useful in the study of pressure ulcer mechanics or other scenarios with similar loading on the skin.

We also looked at changes of mechanical properties in the dermis as well as thickness changes associated with aging. There was little effect on the strain contours and friction coefficients. This is because the simulation is kinematically driven. However, it would be interesting to investigate the response under prescribed loading rather than prescribed indenter movement.

Microrelief aging leads to anisotropic stress patterns during skin-indenter contact

Previous reports have quantified the changes in skin topography or microrelief with aging as well as changes in friction [45, 47, 49, 98–100]. We were therefore poised to evaluate if some of those changes could be explained by the different 3D geometries of the microrelief. Indeed, we see that the microrelief becomes more anisotropic with aging, with the primary skin lines becoming more aligned in the proximal-distal direction in the forearm. Consequently, movement of the indenter leads to more anisotropic stress patterns. Since we use the same material properties the only change we saw was due to the geometry. We saw changes in stress contours as we changed the mechanical properties based on humidity. Wet or dry SC properties mainly

preserved the patterns but altered the magnitude of the shear and normal stresses at the SC. These simulations therefore imply that in designing surfaces in contact with skin it is important to consider the skin topography in three dimensions, as aging will lead to anisotropic stress distributions aligned with the primary skin lines. A related work recently showed that the microrelief can also explain buckling of the skin under lateral compression [46]. However, the work in [46] considered a single adult geometry. Other recent work has further showed than an isotropic microrelief geometry (similar to the 30–40 adult geometry used here) acts as a defect which overall reduces the apparent stiffness of the top layer and favours the onset of wrinkling [101, 102]. Our work therefore also opens new questions, such as the contribution of the increased anisotropy of the aging microrelief to buckling under compression. The surface geometry is not the only thing that changes with aging, but also dermis thickness [45, 84, 103], and dermis mechanical properties [45, 55, 104–106]. We did preliminary work in this direction and we will continue to investigate these changes in more clinically relevant cases in the near future.

In addition to the stress patterns becoming more anisotropic, we also found that the contact area is highly affected by the changes in surface topography with aging. With aging, there is an increase of the plateaus and a reduction of the number of furrows on the surface [57, 58]. Thus, with larger plateau area the contact with the indenter increases in older microrelief geometries.

The primary skin lines in the microrelief influence the global coefficient of friction

This work focused on the interaction with the skin using a local friction coefficient $\mu_l = 0.2$. Previous experimental studies have shown that the interaction of the human skin with different materials and surfaces can show coefficient of friction over a wide range, between 0.059 and 3.7 [44, 107, 108]. Although our analysis does not represent the interaction between the human skin and particular materials, values of $\mu = 0.25$ have been reported for the interaction between calf skin and nitrocellulose [29], $\mu = 0.22$ for the contact between forearm skin and stainless steel [109], $\mu = 0.22$ between forearm and polypropylene and between different body zones and Teflon [27], and $\mu = 0.19$ between forearm skin and steel [44] among other similar values to the local coefficient of friction considered here. Previous work considering rigid indenters and soft substrate showed that the reaction forces on the indenter are not just due to the local friction but that an asymmetric deformation field on the length scale of the indenter can contribute a significant deformation component [33, 34, 86]. In the presence of stronger adhesion interactions, skin at the front of the indenter is compressed while tissue gets stretched behind the indenter movement [110]. Different ranges of material properties, indentation depth, local friction coefficient, and adhesion are needed to see a significant deformation component, which remains to be studied. In our case, keeping all the parameters the same and changing solely from flat to the realistic microrelief surfaces we see a small effect in the coefficient of friction [1]. Looking at the strain contours in a transverse cross section we see that the strains change as the indenter moves on top of the skin and that the contours are asymmetric with respect to the plane defined by indenter movement. However, the features in the strain contours are on the mesoscale, dictated by the ridges and valleys of the microrelief, and while they contribute to the overall oscillation of the tangential forces, there is no significant contribution to a deformation component opposing indenter movement. As a result, the average friction coefficient in the realistic geometries is close to the local friction coefficient, within 13%. In Previous 2D studies by Leyva-Medivil et. al., smaller indenters, with size similar to the topographical features, resulted in a noticeable deformation component that increased friction

[33]. To understand the contribution of deformation and adhesion to the overall frictional response, it is useful to look at the ratio between the skin surface features and the indenter surface features. Consider the ratio $\psi = \phi/R_a$ or $\psi = \phi/R_t$, where ϕ is the diameter of a perfectly smooth indenter, R_a is the arithmetic average height of the skin topography, and R_t is the maximum height of the skin topography (e.g. distance between the deepest valley and the highest peak) [111]. R_a for human skin is about 6.7 μm–46.2 μm and R_t is between 74.03 μm and 84.3 μm [30, 53, 99, 112–114]. Numerical studies performed by Leyva-Mendivil et al [33] considered ψ between 0.8 and 4 and showed a notable influence of the deformation component in the frictional response. In our case ψ is above 31 (base on R_t), which helps to explain the small role of the microrelief deformation on the global friction coefficient.

The more interesting trend of the multivariate analysis was the effect of indenter movement direction with respect to the primary skin lines. This was expected based on the stress analysis, where we saw more anisotropic stress patterns due to the reorientation of skin lines with aging. Nevertheless, the changes are small, especially considering possible variation across individuals. Clearly more work is needed, including adding an adhesion component, testing more indenters with asperities, different local friction coefficients, and a larger set of geometries and boundary conditions.

Limitations

While this work explores the effect of aging in 3D geometries on friction for the first time, it still could improve from a wider set of conditions. It remains to look at other anatomical regions with different skin morphology, topography, mechanical properties, and hair bearing characteristics, such as buttocks or amputation stumps. Mechanical properties of human skin layers were considered as isotropic [33, 46, 76]. More sophisticated material models and more data is also needed in this regard. For instance, several microstructure-based models that account for collagen and elastin fibers and therefore tissue anisotropy have been proposed and should be considered [36]. In fact, the resulting patterns in microrelief and wrinkles with aging are connected to Langer's lines of *in vivo* tension, which themselves reflect the underlying anisotropy of tissue. We ignored adhesion and considered a single local coefficient of friction. Again, a broader parameter range driven by literature reports is needed to include additional variables in a larger study. A single indenter geometry and indentation depth were considered, but other geometries and indentation depths are certainly expected to improve our understanding of skin friction. We only considered three microrelief geometries. While this is clearly an improvement compared to simplified 2D geometries or 3D models of skin that ignore microrelief, additional 3D geometries with microrelief are certainly needed to obtain statistically valid results. At the same time, the changes in microrelief that we see in these three geometries are reflective of the overall changes of microrelief with aging that have been thoroughly reported [42, 47, 56–58]. Lastly, there is certainly no better way of validating the computational model than with additional experiments specifically designed to measure the deformation of the microrelief and the individual skin layers upon contact with an indenter. At the same time, however, this gap in experimental data is also the rationale for our numerical investigation. The proposed finite element model has been carefully constructed based on reported values of individual skin layer mechanics and experimentally measured microrelief geometries. Verification of the model based on mesh convergence and against control simulations of flat geometries were also performed. Observations from our simulations align with previous work, both experimental and computational, while also pose new questions and hypotheses that demand future research.

Conclusions

We show the importance of multi-layered 3D geometries of skin with realistic microrelief and changes with aging. The patterns of the microrelief in 3D are characterized by more anisotropic primary lines with aging, which affect the stress distribution of the skin in contact with the indenter and ultimately affect the friction coefficient depending on orientation. Therefore our results underscore the importance of considering realistic geometries in 3D, especially multi-layered properties and surface topography, for skin mechanics and tribology. Therefore, we expect that our work will enable better design of medical devices and textiles particularly accounting for aging effects.

Supporting information

S1 File. Additional plots and analysis not included in the main text: Principal strains and other strain components during indentation; effect of changes in mechanical properties of the dermis and the stratum corneum; regression analysis; mesh convergence.
(PDF)

Author Contributions

Conceptualization: Juan G. Diosa, Edwin L. Chica, Adrian B. Tepole.

Formal analysis: Juan G. Diosa, Ricardo Moreno, Edwin L. Chica.

Methodology: Adrian B. Tepole.

Resources: Ricardo Moreno, Edwin L. Chica, Junes A. Villarraga.

Supervision: Ricardo Moreno, Edwin L. Chica, Junes A. Villarraga.

Visualization: Juan G. Diosa.

Writing – original draft: Juan G. Diosa.

Writing – review & editing: Ricardo Moreno, Edwin L. Chica, Junes A. Villarraga.

References

1. Abellan MA, Zahouani H, Bergheau JM. Contribution to the Determination of In Vivo Mechanical Characteristics of Human Skin by Indentation Test. Computational and Mathematical Methods in Medicine. 2013. https://doi.org/10.1155/2013/814025 PMID: 24324525
2. Tran HV, Charleux F, Rachik M, Ehrlacher A, Ho Ba Tho MC. In vivo characterization of the mechanical properties of human skin derived from MRI and indentation techniques. Computer Methods in Biomechanics and Biomedical Engineering. 2007; 10(6):401–407. https://doi.org/10.1080/10255840701550287 PMID: 17891674
3. Heide EVD, Zeng X, Masen MA. Skin tribology: Science friction? Friction. 2013; 1(2):130–142. https://doi.org/10.1007/s40544-013-0015-1
4. Zhang S. Modelling non-uniform deformation of human skin in multi-asperity contact. Microsyst Technol. 2018; p. 1–8. https://doi.org/10.1007/s00542-018-3705-9
5. Derler S, Suess J, Rao A, Rotaru GM. Influence of variations in the pressure distribution on the friction of the finger pad. Tribology International. 2013; 63:14–20. https://doi.org/10.1016/j.triboint.2012.03.001
6. Hendriks CP, Franklin SE. Influence of Surface Roughness, Material and Climate Conditions on the Friction of Human Skin. Tribol Lett. 2010; 37(2):361–373. https://doi.org/10.1007/s11249-009-9530-7
7. Schwartz D, Magen YK, Levy A, Gefen A. Effects of humidity on skin friction against medical textiles as related to prevention of pressure injuries. Int Wound J. 2018; 15(6):866–874. https://doi.org/10.1111/iwj.12937 PMID: 29797409

8. Derler S, Rotaru GM, Ke W, Issawi-Frischknecht LE, Kellenberger P, Scheel-Sailer A, et al. Microscopic contact area and friction between medical textiles and skin. Journal of the Mechanical Behavior of Biomedical Materials. 2014; 38:114–125. https://doi.org/10.1016/j.jmbbm.2014.06.014 PMID: 25047353

9. Kottner J, Black J, Call E, Gefen A, Santamaria N. Microclimate: A critical review in the context of pressure ulcer prevention. Clinical Biomechanics. 2018; 59:62–70. https://doi.org/10.1016/j.clinbiomech.2018.09.010 PMID: 30199821

10. Li W, Pang Q, Lu M, Liu Y, Zhou ZR. Rehabilitation and adaptation of lower limb skin to friction trauma during friction contact. Wear. 2015; 332-333:725–733. https://doi.org/10.1016/j.wear.2015.01.045

11. Baussan E, Bueno MA, Rossi RM, Derler S. Experiments and modelling of skin-knitted fabric friction. Wear. 2010; 268(9):1103–1110. https://doi.org/10.1016/j.wear.2010.01.010

12. Carlson JM. Functional limitations from pain caused by repetitive loading on the skin: A review and discussion for practitioners, with new data for limiting friction loads. JPO: Journal of Prosthetics and Orthotics. 2006; 18(4):93–103.

13. Baussan E, Bueno M, Rossi R, Derler S. Analysis of current running sock structures with regard to blister prevention. Textile Research Journal. 2013; 83(8):836–848. https://doi.org/10.1177/0040517512461698

14. Meulenbelt H, Geertzen J, Jonkman M, Dijkstra P. Skin Problems of the Stump in Lower Limb Amputees: 1. A Clinical Study. Acta Dermato Venereologica. 2011; 91(2):173–177. https://doi.org/10.2340/00015555-1040 PMID: 21290085

15. Meulenbelt HE, Geertzen JH, Jonkman MF, Dijkstra PU. Determinants of skin problems of the stump in lower-limb amputees. Arch Phys Med Rehabil. 2009; 90(1):74–81. https://doi.org/10.1016/j.apmr.2008.07.015 PMID: 19154832

16. Leung IPH, Fleming L, Walton K, Barrans S, Ousey K. Development of a model to demonstrate the effects of friction and pressure on skin in relation to pressure ulcer formation. Wear. 2017; 376-377:266–271. https://doi.org/10.1016/j.wear.2016.11.026

17. Zheng YP, Mak AF, Leung AK. State-of-the-art methods for geometric and biomechanical assessments of residual limbs: a review. J Rehabil Res Dev. 2001; 38(5):487–504. PMID: 11732827

18. Zhang M, Mak AFT. In vivo friction properties of human skin. Prosthetics and Orthotics International. 1999; 23(2):135–141. https://doi.org/10.3109/03093649909071625 PMID: 10493141

19. Sree VD, Rausch MK, Tepole AB. Towards understanding pressure ulcer formation: coupling an inflammation regulatory network to a tissue scale finite element model. Mechanics Research Communications. 2019; 97:80–88. https://doi.org/10.1016/j.mechrescom.2019.05.003

20. Sree VD, Rausch MK, Tepole AB. Linking microvascular collapse to tissue hypoxia in a multiscale model of pressure ulcer initiation. Biomechanics and modeling in mechanobiology. 2019; 18(6):1947–1964. https://doi.org/10.1007/s10237-019-01187-5 PMID: 31203488

21. Sopher R, Gefen A. Effects of skin wrinkles, age and wetness on mechanical loads in the stratum corneum as related to skin lesions. Med Biol Eng Comput. 2011; 49(1):97–105. https://doi.org/10.1007/s11517-010-0673-3 PMID: 20717736

22. Stojadinovic O, Minkiewicz J, Sawaya A, Bourne JW, Torzilli P, Vaccari JPdR, et al. Deep Tissue Injury in Development of Pressure Ulcers: A Decrease of Inflammasome Activation and Changes in Human Skin Morphology in Response to Aging and Mechanical Load. PLOS ONE. 2013; 8(8):e69223. https://doi.org/10.1371/journal.pone.0069223 PMID: 23967056

23. Silver-Thorn MB, Steege JW, Childress DS. A review of prosthetic interface stress investigations. J Rehabil Res Dev. 1996; 33(3):253–266. PMID: 8823673

24. Mao X, Yamada Y, Akiyama Y, Okamoto S, Yoshida K. Safety verification method for preventing friction blisters during utilization of physical assistant robots. Advanced Robotics. 2017; 31(13):680–694. https://doi.org/10.1080/01691864.2017.1318716

25. Veijgen NK, Masen MA, van der Heide E. Variables influencing the frictional behaviour of in vivo human skin. Journal of the Mechanical Behavior of Biomedical Materials. 2013. https://doi.org/10.1016/j.jmbbm.2013.02.009 PMID: 23796756

26. Veijgen NK, van der Heide E, Masen MA. A multivariable model for predicting the frictional behaviour and hydration of the human skin. Skin Research and Technology. 2013; 19(3):330–338. https://doi.org/10.1111/srt.12053 PMID: 23441726

27. Cua AB, Wilhelm KP, Maibach HI. Frictional properties of human skin: Relation to age, sex and anatomical region, stratum corneum hydration and transepidermal water loss. British Journal of Dermatology. 1990; 123(4):473–479. https://doi.org/10.1111/j.1365-2133.1990.tb01452.x PMID: 2095179

28. Veijgen NKa, Masen MAa, Van Der Heide Eab. Relating friction on the human skin to the hydration and temperature of the skin. Tribology Letters. 2013; 49(1):251–262. https://doi.org/10.1007/s11249-012-0062-1

29. Abdel-Aal HA, El Mansori M, Zahouani H. A comparative study of frictional response of shed snakeskin and human skin. Wear. 2017; 376–377, Part A:281–294. https://doi.org/10.1016/j.wear.2016.12.055

30. Klaassen M, de Vries EG, Masen MA. Friction in the contact between skin and a soft counter material: Effects of hardness and surface finish. Journal of the Mechanical Behavior of Biomedical Materials. 2019; 92:137–143. https://doi.org/10.1016/j.jmbbm.2019.01.006 PMID: 30685727

31. Derler S, Gerhardt LC, Lenz A, Bertaux E, Hadad M. Friction of human skin against smooth and rough glass as a function of the contact pressure. Tribology International. 2009; 42(11–12):1565–1574. https://doi.org/10.1016/j.triboint.2008.11.009

32. Xing M, Zhong W, Pan N. 20—Biomechanics in skin/clothing interactions. In: Pan N, Sun G, editors. Functional Textiles for Improved Performance, Protection and Health. Woodhead Publishing Series in Textiles. Woodhead Publishing; 2011. p. 462–488. Available from: http://www.sciencedirect.com/science/article/pii/B9781845697235500204.

33. Leyva-Mendivil MF, Lengiewicz J, Limbert G. Skin friction under pressure. The role of micromechanics. Surf Topogr: Metrol Prop. 2018; 6(1):014001. https://doi.org/10.1088/2051-672X/aaa2d4

34. Leyva-Mendivil MF, Lengiewicz J, Page A, Bressloff NW, Limbert G. Skin Microstructure is a Key Contributor to Its Friction Behaviour. Tribol Lett. 2017; 65(1):12. https://doi.org/10.1007/s11249-016-0794-4 PMID: 32009774

35. Boyer G, Molimard J, Ben Tkaya M, Zahouani H, Pericoi M, Avril S. Assessment of the in-plane biomechanical properties of human skin using a finite element model updating approach combined with an optical full-field measurement on a new tensile device. Journal of the Mechanical Behavior of Biomedical Materials. 2013; 27:273–282. https://doi.org/10.1016/j.jmbbm.2013.05.024 PMID: 23867292

36. Limbert Georges. Mathematical and computational modelling of skin biophysics: a review. Proceedings of the Royal Society A: Mathematical, Physical and Engineering Sciences. 2017; 473 (2203):20170257. https://doi.org/10.1098/rspa.2017.0257

37. Johnson SA, Gorman DM, Adams MJ, Briscoe BJ. The friction and lubrication of human stratum corneum. In: Dowson D, Taylor CM, Childs THC, Godet M, Dalmaz G, editors. Tribology Series. vol. 25 of Thin Films in Tribology. Elsevier; 1993. p. 663–672. Available from: http://www.sciencedirect.com/science/article/pii/S016789220870419X.

38. Geerligs M, van Breemen L, Peters G, Ackermans P, Baaijens F, Oomens C. In vitro indentation to determine the mechanical properties of epidermis. Journal of Biomechanics. 2011; 44(6):1176–1181. https://doi.org/10.1016/j.jbiomech.2011.01.015 PMID: 21296353

39. Wu KS, van Osdol WW, Dauskardt RH. Mechanical properties of human stratum corneum: Effects of temperature, hydration, and chemical treatment. Biomaterials. 2006; 27(5):785–795. https://doi.org/10.1016/j.biomaterials.2005.06.019 PMID: 16095683

40. Ní Annaidh A, Bruyère K, Destrade M, Gilchrist MD, Otténio M. Characterization of the anisotropic mechanical properties of excised human skin. Journal of the Mechanical Behavior of Biomedical Materials. 2012; 5(1):139–148. https://doi.org/10.1016/j.jmbbm.2011.08.016 PMID: 22100088

41. Laiacona D, Cohen J, Coulon K, Lipsky ZW, Maiorana C, Boltyanskiy R, et al. Non-invasive in vivo quantification of human skin tension lines. Acta biomaterialia. 2019; 88:141–148. https://doi.org/10.1016/j.actbio.2019.02.003 PMID: 30735808

42. Zahouani H, Djaghloul M, Vargiolu R, Mezghani S, Mansori MEL. Contribution of human skin topography to the characterization of dynamic skin tension during senescence: morpho-mechanical approach. Journal of Physics: Conference Series. 2014; 483:012012. https://doi.org/10.1088/1742-6596/483/1/012012

43. Benítez JM, Montáns FJ. The mechanical behavior of skin: Structures and models for the finite element analysis. Computers & Structures. 2017; 190:75–107. https://doi.org/10.1016/j.compstruc.2017.05.003

44. Derler S, Gerhardt LC. Tribology of Skin: Review and Analysis of Experimental Results for the Friction Coefficient of Human Skin. Tribol Lett. 2012; 45(1):1–27. https://doi.org/10.1007/s11249-011-9854-y

45. Limbert G, Masen MA, Pond D, Graham HK, Sherratt MJ, Jobanputra R, et al. Biotribology of the ageing skin—Why we should care. Biotribology. 2019; 17:75–90. https://doi.org/10.1016/j.biotri.2019.03.001

46. Limbert G, Kuhl E. On skin microrelief and the emergence of expression micro-wrinkles. Soft Matter. 2018; 14(8):1292–1300. https://doi.org/10.1039/C7SM01969F PMID: 29319711

47. Zou Y, Song E, Jin R. Age-dependent changes in skin surface assessed by a novel two-dimensional image analysis. Skin Research and Technology. 2009; 15(4):399–406. https://doi.org/10.1111/j.1600-0846.2009.00377.x PMID: 19832949

48. Derler S, Schrade U, Gerhardt LC. Tribology of human skin and mechanical skin equivalents in contact with textiles. Wear. 2007; 263(7–12):1112–1116. https://doi.org/10.1016/j.wear.2006.11.031

49. Zahouani H, Boyer G, Pailler-Mattei C, Ben Tkaya M, Vargiolu R. Effect of human ageing on skin rheology and tribology. Wear. 2011; 271(9–10):2364–2369. https://doi.org/10.1016/j.wear.2011.02.024

50. Gerhardt LCab, Strässle Va, Lenz Aa, Spencer NDb, Derler Sa. Influence of epidermal hydration on the friction of human skin against textiles. Journal of the Royal Society Interface. 2008; 5(28):1317–1328. https://doi.org/10.1098/rsif.2008.0034 PMID: 18331977

51. Persson BNJa, Kovalev Ab, Gorb SNb. Contact mechanics and friction on dry and wet human skin. Tribology Letters. 2013; 50(1):17–30. https://doi.org/10.1007/s11249-012-0053-2

52. Klaassen M, de Vries EG, Masen MA. The static friction response of non-glabrous skin as a function of surface energy and environmental conditions. Biotribology. 2017; 11:124–131. https://doi.org/10.1016/j.biotri.2017.05.004

53. Morales-Hurtado M, de Vries EG, Peppelman M, Zeng X, van Erp PEJ, van der Heide E. On the role of adhesive forces in the tribo-mechanical performance of ex vivo human skin. Tribology International. 2017; 107:25–32. https://doi.org/10.1016/j.triboint.2016.11.006

54. Klaassen M, Schipper DJ, Masen MA. Influence of the relative humidity and the temperature on the in-vivo friction behaviour of human skin. Biotribology. 2016; 6:21–28. https://doi.org/10.1016/j.biotri.2016.03.003

55. Pailler-Mattei C, Debret R, Vargiolu R, Sommer P, Zahouani H. In vivo skin biophysical behaviour and surface topography as a function of ageing. Journal of the Mechanical Behavior of Biomedical Materials. 2013; 28:474–483. https://doi.org/10.1016/j.jmbbm.2013.04.008 PMID: 23664827

56. Akazaki S, Nakagawa H, Kazama H, Osanai O, Kawai M, Takema Y, et al. Age-related changes in skin wrinkles assessed by a novel three-dimensional morphometric analysis. British Journal of Dermatology. 2002; 147(4):689–695. https://doi.org/10.1046/j.1365-2133.2002.04874.x PMID: 12366414

57. Boyer Ga, Laquièze La, Le Bot Aa, Laquièze Sb, Zahouani Ha. Dynamic indentation on human skin in vivo: Ageing effects. Skin Research and Technology. 2009; 15(1):55–67. https://doi.org/10.1111/j.1600-0846.2008.00324.x

58. Lagarde JM, Rouvrais C, Black D. Topography and anisotropy of the skin surface with ageing. Skin Research and Technology. 2005; 11(2):110–119. https://doi.org/10.1111/j.1600-0846.2005.00096.x PMID: 15807809

59. Meador WD, Sugerman GP, Story HM, Seifert AW, Bersi MR, Tepole AB, et al. The regional-dependent biaxial behavior of young and aged mouse skin: A detailed histomechanical characterization, residual strain analysis, and constitutive model. Acta Biomaterialia. 2020; 101:403–413. https://doi.org/10.1016/j.actbio.2019.10.020 PMID: 31614209

60. Lynch B, Bonod-Bidaud C, Ducourthial G, Affagard JS, Bancelin S, Psilodimitrakopoulos S, et al. How aging impacts skin biomechanics: a multiscale study in mice. Scientific reports. 2017; 7(1):1–10. https://doi.org/10.1038/s41598-017-13150-4 PMID: 29061975

61. Comaish S, Bottoms E. The Skin and Friction: Deviations from Amonton's Laws, and the Effects of Hydration and Lubrication. British Journal of Dermatology. 1971; 84(1):37–43. https://doi.org/10.1111/j.1365-2133.1971.tb14194.x PMID: 5573184

62. Zahouani H, Vargiolu R, Boyer G, Pailler-Mattei C, Laquièze L, Mavon A. Friction noise of human skin in vivo. Wear. 2009; 267(5-8):1274–1280. https://doi.org/10.1016/j.wear.2009.03.007

63. Derler S, Rossi R, Rotaru GM. Understanding the variation of friction coefficients of human skin as a function of skin hydration and interfacial water films. Proceedings of the Institution of Mechanical Engineers, Part J: Journal of Engineering Tribology. 2015; 229(3):285–293. https://doi.org/10.1177/1350650114527922

64. Hurtado MM, Peppelman M, Zeng X, van Erp PEJ, Van Der Heide E. Tribological behaviour of skin equivalents and ex-vivo human skin against the material components of artificial turf in sliding contact. Tribology International. 2016; 102:103–113. https://doi.org/10.1016/j.triboint.2016.05.018

65. Ní Annaidh A, f KBe, Destrade Mag, Gilchrist MDa, Maurini Cbc, Otténio Mdef, et al. Automated estimation of collagen fibre dispersion in the dermis and its contribution to the anisotropic behaviour of skin. Annals of Biomedical Engineering. 2012; 40(8):1666–1678. https://doi.org/10.1007/s10439-012-0542-3 PMID: 22427196

66. Flynn C, Taberner A, Nielsen P. Mechanical characterisation of in vivo human skin using a 3D force-sensitive micro-robot and finite element analysis. Biomech Model Mechanobiol. 2011; 10(1):27–38. https://doi.org/10.1007/s10237-010-0216-8 PMID: 20429025

67. Kvistedal YA, Nielsen PMF. Estimating material parameters of human skin in vivo. Biomech Model Mechanobiol. 2009; 8(1):1–8. https://doi.org/10.1007/s10237-007-0112-z PMID: 18040732

68. Tonge TK, Voo LM, Nguyen TD. Full-field bulge test for planar anisotropic tissues: Part II—A thin shell method for determining material parameters and comparison of two distributed fiber modeling

approaches. Acta Biomaterialia. 2013; 9(4):5926–5942. https://doi.org/10.1016/j.actbio.2012.11.034 PMID: 23220451

69. Delalleau A, Josse G, Lagarde JM, Zahouani H, Bergheau JM. A nonlinear elastic behavior to identify the mechanical parameters of human skin in vivo. Skin Research and Technology. 2008; 14(2):152–164. https://doi.org/10.1111/j.1600-0846.2007.00269.x PMID: 18412557

70. Liang Xa, Boppart SAb. Biomechanical properties of in vivo human skin from dynamic optical coherence elastography. IEEE Transactions on Biomedical Engineering. 2010; 57(4):953–959. https://doi.org/10.1109/TBME.2009.2033464

71. Khatyr F, Imberdis C, Vescovo P, Varchon D, Lagarde JM. Model of the viscoelastic behaviour of skin in vivo and study of anisotropy. Skin Research and Technology. 2004; 10(2):96–103. https://doi.org/10.1111/j.1600-0846.2004.00057.x PMID: 15059176

72. Abellan MA, Bergheau JM, Zahouani H. Comparison of different viscoelastic models for the characterisation of mechanical properties of human skin in vivo by indentation test. Computer Methods in Biomechanics and Biomedical Engineering. 2014; 17(sup1):22–23. https://doi.org/10.1080/10255842.2014.931077 PMID: 25074145

73. Lapeer RJ, Gasson PD, Karri V. Simulating plastic surgery: From human skin tensile tests, through hyperelastic finite element models to real-time haptics. Progress in Biophysics and Molecular Biology. 2010; 103(2-3):208–216. https://doi.org/10.1016/j.pbiomolbio.2010.09.013 PMID: 20869388

74. Groves RB, Coulman SA, Birchall JC, Evans SL. An anisotropic, hyperelastic model for skin: Experimental measurements, finite element modelling and identification of parameters for human and murine skin. Journal of the Mechanical Behavior of Biomedical Materials. 2013; 18:167–180. https://doi.org/10.1016/j.jmbbm.2012.10.021 PMID: 23274398

75. Flynn C, McCormack BAO. Simulating the wrinkling and aging of skin with a multi-layer finite element model. Journal of Biomechanics. 2010; 43(3):442–448. https://doi.org/10.1016/j.jbiomech.2009.10.007 PMID: 19889419

76. Groves RBa, Coulman SAb, Birchall JCb, Evans SLa. Quantifying the mechanical properties of human skin to optimise future microneedle device design. Computer Methods in Biomechanics and Biomedical Engineering. 2012; 15(1):73–82. https://doi.org/10.1080/10255842.2011.596481 PMID: 21749225

77. Crichton ML, Donose BC, Chen X, Raphael AP, Huang H, Kendall MAF. The viscoelastic, hyperelastic and scale dependent behaviour of freshly excised individual skin layers. Biomaterials. 2011; 32(20):4670–4681. https://doi.org/10.1016/j.biomaterials.2011.03.012 PMID: 21458062

78. Zahouani Ha, Pailler-Mattei Ca, Sohm Bb, Vargiolu Ra, Cenizo Vb, Debret Rc. Characterization of the mechanical properties of a dermal equivalent compared with human skin in vivo by indentation and static friction tests. Skin Research and Technology. 2009; 15(1):68–76. https://doi.org/10.1111/j.1600-0846.2008.00329.x

79. Lévêque JL, Audoly B. Influence of Stratum Corneum on the entire skin mechanical properties, as predicted by a computational skin model. Skin Research and Technology. 2013; 19(1):42–46. https://doi.org/10.1111/j.1600-0846.2012.00664.x PMID: 22925192

80. Hwang K, Kim H, Kim DJ. Thickness of skin and subcutaneous tissue of the free flap donor sites: A histologic study. Microsurgery. 2016; 36(1):54–58. https://doi.org/10.1002/micr.30000 PMID: 26529557

81. Kligman AM, Zheng P, Lavker RM. The anatomy and pathogenesis of wrinkles. British Journal of Dermatology. 1985; 113(1):37–42. https://doi.org/10.1111/j.1365-2133.1985.tb02042.x PMID: 4015970

82. Leyva-Mendivil MF, Page A, Bressloff NW, Limbert G. A mechanistic insight into the mechanical role of the stratum corneum during stretching and compression of the skin. Journal of the Mechanical Behavior of Biomedical Materials. 2015; 49:197–219. https://doi.org/10.1016/j.jmbbm.2015.05.010 PMID: 26042766

83. Pavšelj N, Mitar M, Hart FX, Miklavčič D. Characterization of the mechanical behavior of human skin by means of impedance spectroscopy. Journal of Physics: Conference Series. 2010; 224(1):012131. https://doi.org/10.1088/1742-6596/224/1/012131

84. Pond D, McBride AT, Davids LM, Reddy BD, Limbert G. Microstructurally-based constitutive modelling of the skin—Linking intrinsic ageing to microstructural parameters. Journal of Theoretical Biology. 2018; 444:108–123. https://doi.org/10.1016/j.jtbi.2018.01.014 PMID: 29407269

85. Weickenmeier J, Jabareen M, Mazza E. Suction based mechanical characterization of superficial facial soft tissues. Journal of biomechanics. 2015; 48(16):4279–4286. https://doi.org/10.1016/j.jbiomech.2015.10.039 PMID: 26584965

86. Stupkiewicz S, Lewandowski MJ, Lengiewicz J. Micromechanical analysis of friction anisotropy in rough elastic contacts. International Journal of Solids and Structures. 2014; 51(23):3931–3943. https://doi.org/10.1016/j.ijsolstr.2014.07.013

87. Maas SA, Ellis BJ, Ateshian GA, Weiss JA. FEBio: Finite Elements for Biomechanics. J Biomech Eng. 2012; 134(1):011005–011005–10. https://doi.org/10.1115/1.4005694 PMID: 22482660

88. Asserin J, Zahouani H, Humbert P, Couturaud V, Mougin D. Measurement of the friction coefficient of the human skin in vivo: Quantification of the cutaneous smoothness. Colloids and Surfaces B: Biointerfaces. 2000; 19(1):1–12. https://doi.org/10.1016/S0927-7765(99)00169-1

89. Li W, Kong M, Liu XD, Zhou ZR. Tribological behavior of scar skin and prosthetic skin in vivo. Tribology International. 2008; 41(7):640–647. https://doi.org/10.1016/j.triboint.2007.11.009

90. Tang W, Ge Sr, Zhu H, Cao Xc, Li N. The Influence of Normal Load and Sliding Speed on Frictional Properties of Skin. Journal of Bionic Engineering. 2008; 5(1):33–38. https://doi.org/10.1016/S1672-6529(08)60004-9

91. Pailler-Mattei C, Bec S, Zahouani H. In vivo measurements of the elastic mechanical properties of human skin by indentation tests. Medical Engineering & Physics. 2008; 30(5):599–606. https://doi.org/10.1016/j.medengphy.2007.06.011 PMID: 17869160

92. Delalleau A, Josse G, Lagarde JM, Zahouani H, Bergheau JM. Characterization of the mechanical properties of skin by inverse analysis combined with the indentation test. Journal of Biomechanics. 2006; 39(9):1603–1610. https://doi.org/10.1016/j.jbiomech.2005.05.001 PMID: 15990103

93. Hendriks FM, Brokken D, Oomens CWJ, Baaijens FPT, Horsten J. Mechanical Properties of Different Layers of Human Skin. Internal Poster (http://yp.bmt.tue.nl/pdfs/249.pdf), Department of Biomedical Engineering, Eindhoven University of Technology. 2000.

94. van Kuilenburg J, Masen MA, van der Heide E. Contact modelling of human skin: What value to use for the modulus of elasticity? Proceedings of the institution of mechanical engineers, Part J: Journal of Engineering Tribology. 2013; 227(4):349–361. https://doi.org/10.1177/1350650112463307

95. Liu X, Cleary J, German G. The global mechanical properties and multi-scale failure mechanics of heterogeneous human stratum corneum. Acta biomaterialia. 2016; 43:78–87. https://doi.org/10.1016/j.actbio.2016.07.028 PMID: 27431879

96. Levy A, Kopplin K, Gefen A. Device-related pressure ulcers from a biomechanical perspective. Journal of Tissue Viability. 2017; 26(1):57–68. https://doi.org/10.1016/j.jtv.2016.02.002 PMID: 26927980

97. Hoogendoorn I, Reenalda J, Koopman BFJM, Rietman JS. The effect of pressure and shear on tissue viability of human skin in relation to the development of pressure ulcers: a systematic review. Journal of Tissue Viability. 2017; 26(3):157–171. https://doi.org/10.1016/j.jtv.2017.04.003 PMID: 28457615

98. Djaghloul M, Abdouni A, Thieulin C, Zahouani H. Wave propagation as a marker of structural and topographic properties of human skin. Surf Topogr: Metrol Prop. 2018; 6(2):024008. https://doi.org/10.1088/2051-672X/aabfb2

99. Thieulin C, Pailler-Mattei C, Abdouni A, Djaghloul M, Zahouani H. Mechanical and topographical anisotropy for human skin: Ageing effect. Journal of the Mechanical Behavior of Biomedical Materials. 2020; 103:103551. https://doi.org/10.1016/j.jmbbm.2019.103551 PMID: 32090946

100. Djaghloul M, Morizot F, Zahouani H. Elastic wave induced by friction as a signature of human skin ageing and gender effect. Skin Research and Technology. 2016; 22(3):349–355. https://doi.org/10.1111/srt.12272 PMID: 26566792

101. Shiihara Y, Sato M, Hara Y, Iwai I, Yoshikawa N. Microrelief suppresses large wrinkling appearance: an in silico study. Skin Research and Technology. 2015; 21(2):184–191. https://doi.org/10.1111/srt.12175 PMID: 25470358

102. Chavoshnejad P, More S, Razavi MJ. From surface microrelief to big wrinkles in skin: A mechanical in-silico model. Extreme Mechanics Letters. 2020; 36:100647. https://doi.org/10.1016/j.eml.2020.100647

103. Zhao Y, Feng B, Lee J, Lu N, Pierce DM. A multi-layered computational model for wrinkling of human skin predicts aging effects. Journal of the Mechanical Behavior of Biomedical Materials. 2020; 103:103552. https://doi.org/10.1016/j.jmbbm.2019.103552 PMID: 32090947

104. Escoffier C, De Rigal J, Rochefort A, Vasselet R, Leveque JL, Agache PG. Age-related mechanical properties of human skin: An in vivo study. Journal of Investigative Dermatology. 1989; 93(3):353–357. https://doi.org/10.1016/0022-202X(89)90058-4 PMID: 2768836

105. Krueger N, Luebberding S, Oltmer M, Streker M, Kerscher M. Age-related changes in skin mechanical properties: a quantitative evaluation of 120 female subjects. Skin Research and Technology. 2011; 17(2):141–148. https://doi.org/10.1111/j.1600-0846.2010.00486.x PMID: 21281361

106. Luebberding S, Krueger N, Kerscher M. Mechanical properties of human skin in vivo: A comparative evaluation in 300 men and women. Skin Research and Technology. 2013. https://doi.org/10.1111/srt.12094 PMID: 23889488

107. Li W, Liu XD, Cai ZB, Zheng J, Zhou ZR. Effect of prosthetic socks on the frictional properties of residual limb skin. Wear. 2011; 271(11):2804–2811. https://doi.org/10.1016/j.wear.2011.05.032

108. Pailler-Mattei C, Nicoli S, Pirot F, Vargiolu R, Zahouani H. A new approach to describe the skin surface physical properties in vivo. Colloids and Surfaces B: Biointerfaces. 2009; 68(2):200–206. https://doi.org/10.1016/j.colsurfb.2008.10.005 PMID: 19042108

109. Chen CY, Yu CA, Hong TF, Chung YL, Li WL. Contact and frictional properties of stratum corneum of human skin. Biosurface and Biotribology. 2015; 1(1):62–70. https://doi.org/10.1016/j.bsbt.2015.02.001

110. Kwiatkowska M, Franklin SE, Hendriks CP, Kwiatkowski K. Friction and deformation behaviour of human skin. Wear. 2009; 267(5–8):1264–1273. https://doi.org/10.1016/j.wear.2008.12.030

111. Gadelmawla ES, Koura MM, Maksoud TMA, Elewa IM, Soliman HH. Roughness parameters. Journal of Materials Processing Technology. 2002; 123(1):133–145. https://doi.org/10.1016/S0924-0136(02)00060-2

112. Piérard GE, Uhoda I, Piérard-Franchimont C. From skin microrelief to wrinkles. An area ripe for investigation. Journal of cosmetic dermatology. 2003; 2(1):21–28. https://doi.org/10.1111/j.1473-2130.2003.00012.x PMID: 17156045

113. Antosik AK, Piatek A, Wilpiszewska K. Carboxymethylated starch and cellulose derivatives-based film as human skin equivalent for adhesive properties testing. Carbohydrate Polymers. 2019; 222:115014. https://doi.org/10.1016/j.carbpol.2019.115014 PMID: 31320045

114. Dabrowska AK, Spano F, Derler S, Adlhart C, Spencer ND, Rossi RM. The relationship between skin function, barrier properties, and body-dependent factors. Skin Research and Technology. 2018; 24(2):165–174. https://doi.org/10.1111/srt.12424 PMID: 29057509